Sources, transport and deposition of iron in the global atmosphere

Rong Wang[1,2,3], Yves Balkanski[1,3], Olivier Boucher[4], Laurent Bopp[1], Adrian Chappell[5], Philippe Ciais[1,3], Didier Hauglustaine[1], Josep Peñuelas[6,7], Shu Tao[2,3]

[1] Laboratoire des Sciences du Climat et de l'Environnement, CEA CNRS UVSQ, Gif-sur-Yvette, France

[2] Laboratory for Earth Surface Processes, College of Urban and Environmental Sciences, Peking University, Beijing, China

[3] Sino-French Institute for Earth System Science, College of Urban and Environmental Sciences, Peking University, Beijing, China

[4] Laboratoire de Météorologie Dynamique, IPSL/CNRS, Université Pierre et Marie Curie, France

[5] CSIRO Land & Water National Research Flagship, GPO Box 1666, Canberra, ACT 2601, Australia

[6] Consejo Superior de Investigaciones Científicas, Global Ecology Unit CREAF-CEAB-UAB, Spain

[7] Centre de Recerca Ecologica i Aplicacions Forestals, Spain

Correspondence to: R. Wang (Rong.Wang@lsce.ipsl.fr)

Abstract

Atmospheric deposition of iron (Fe) plays an important role in controlling oceanic primary productivity. However, the sources of Fe in the atmosphere are not well understood. In particular, the combustion sources of Fe and the subsequent deposition to the oceans have been accounted for in only few ocean biogeochemical models of the carbon cycle. Here we used a mass-balance method to estimate the emissions of Fe from the combustion of fossil fuels and biomass by accounting for the Fe contents in fuel and the partitioning of Fe during combustion. The emissions of Fe attached to aerosols from combustion sources were estimated by particle size, and their uncertainties were quantified by a Monte Carlo simulation. The emissions of Fe from mineral sources were estimated using the latest soil mineralogical database to date. As a result, the total Fe emissions from combustion averaged for 1960-2007 were estimated to be 5.3 Tg yr^{-1} (90% confidence of 2.3 to 12.1). Of these emissions, 1, 27 and 72% were emitted in particles < 1 μm (PM_1), 1-10 μm (PM_{1-10}), and > 10 μm ($PM_{>10}$), respectively, compared to a total Fe emission from mineral dust of 41.0 Tg yr^{-1} in a log-normal distribution with a mass median diameter of 2.5 μm and a geometric standard deviation of 2. For combustion sources, different temporal trends were found in fine and medium-to-coarse particles, with a notable increase in Fe emissions in PM_1 since 2000 due to an increase in Fe emission from motor vehicles (from 0.008 to 0.0103 Tg yr^{-1} in 2000 and 2007, respectively). These emissions have been introduced in a global 3-D transport model run at a spatial resolution of of 0.94° latitude by 1.28° longitude to evaluate our estimation of Fe emissions. The modelled Fe concentrations as monthly means were compared with the monthly (57 sites) or daily (768 sites) measured concentrations at a total of 825 sampling stations. The deviation between modelled and observed Fe concentrations attached to aerosols at the surface was within a factor of two at most sampling stations, and the deviation was within a factor of 1.5 at sampling stations dominated by combustion sources. We analyzed the relative contribution of combustion sources to total Fe concentrations over different regions of the world. The new mineralogical database led to a modest improvement in the simulation relative to station data even in dust dominated regions, but could provide useful information on the chemical forms of Fe in dust for coupling with ocean biota models. We estimated a total Fe deposition sink of 8.4 Tg yr^{-1} over global oceans, 7% of which originated from the combustion sources. Our central estimates of Fe emissions from fossil fuel combustion (mainly from coal) are generally higher than those in previous studies, although they are within the uncertainty range of our estimates. In particular, the higher than previously estimated Fe emission from coal combustion implies a larger atmospheric anthropogenic input of soluble Fe to the northern Atlantic and northern Pacific Oceans, which is expected to enhance the biological carbon pump in those regions.

1 Introduction

Sea-water dissolved iron (Fe) concentration is a primary factor that limits or co-limits the growth of phytoplankton in large regions of the global oceans (Martin et al., 1991; Moore et al., 2013). As such, Fe availability influences the transfer and sequestration of carbon into the deep ocean (Boyd et al., 2000; Moore et al., 2004). Both ice-core and marine-sediment records indicate high rates of aeolian dust and hence Fe supply to the oceans at the Last Glacial Maximum, implying a potential link between Fe availability, marine productivity, atmospheric CO_2 and climate through Fe fertilization (Martin, 1990; Ridgwell and Watson, 2002). Over the Industrial Era, the increase of Fe deposition in dust was estimated to be responsible for a decrease of atmospheric CO_2 by 4 ppm (Mahowald et al., 2011), with a large uncertainty.

Atmospheric deposition provides an important source of Fe to the marine biota (Martin, 1990; Duce and Tindale, 1991; Johnson et al., 1997; Fung et al., 2000; Gao et al., 2001; Conway and John, 2014). Early studies of the effects of Fe fertilization, however, mostly focused on aeolian dust sources (Hand et al., 2004; Luo et al., 2003; Gregg et al., 2003; Moore et al., 2004; Mahowald et al., 2005; Fan et al., 2006). Observed concentrations of soluble Fe were not properly captured by the models simulating the atmospheric transport, chemical processing and deposition of Fe in aerosols (Hand et al., 2004; Luo et al., 2005; Fan et al., 2006), thus suggesting the existence of other sources. Guieu et al. (2005) proposed that the burning of biomass could be an additional source of soluble Fe in the Ligurian Sea. Chuang et al. (2005) reported that soluble Fe observed at an atmospheric deposition measurement station in Korea was not dominated by mineral sources, even during dust storms. Sedwick et al. (2007) hypothesized that the anthropogenic emissions of Fe from combustion could play a significant role in the atmospheric input of bioavailable Fe to the surface of the Atlantic Ocean. However, few global models have accounted for the impact of Fe from combustion on the open-ocean biogeochemistry (Krishnamurthy et al., 2009; Okin et al., 2011), due to large uncertainties for the sources and chemical forms of Fe from combustion.

The first estimate of Fe emissions from fossil fuels and biomass burning reported a total Fe emission of 1.7 Tg yr^{-1} (Luo et al., 2008). Ito and Feng (2010) subsequently obtained a lower estimate of 1.2 Tg yr^{-1}. By applying a high emission factor of Fe from ships and accounting for a large Fe solubility from oil fly ash, Ito (2013) later derived the same total Fe emission of 1.2 Tg yr^{-1}, but with a significant contribution by shipping to soluble Fe deposition over the northern Pacific Ocean and the East China Sea.. These authors suggested that more work was required to reduce the uncertainty in Fe emissions, particularly from the combustion of petroleum and biomass.

The mineral composition of dust is a key factor in the chemical forms of Fe, and it determines the solubility and thus the bioavailability of Fe. Nickovic et al. (2012) developed a global data set to represent the mineral composition of soil in arid and semi-arid areas. This mineralogical data set improved the agreement between simulated and measured concentrations of soluble Fe (Nickovic et al., 2013; Ito and Xu, 2014). More recently, Journet et al. (2014) developed a new data set of soil mineralogy (including soil Fe content) covering most dust source regions of the world at a resolution of 0.5° × 0.5°, with the aim to improve the modelling of the chemical forms of Fe in dust.

In this study, we estimated the emissions of Fe from combustion sources for 222 countries / territories over 1960 to 2007 period using a new method based on Fe content of fuel and Fe budget during combustion. We re-estimated Fe emissions from mineral sources based on the latest mineralogical database. Our estimates of

Fe sources were evaluated by an atmospheric transport model at a fine resolution. The impact of the estimated combustion-related and mineral emissions of Fe on the model-data misfits at 825 stations measuring Fe concentration in surface aerosol and 30 stations measuring Fe deposition was investigated for different regions and stations.

2 Data and Methodology

2.1 Emissions of Fe from combustion sources

A global emission inventory of Fe from combustion was developed, covering 222 countries / territories and the 1960 to 2007 period. The sources of Fe emission included the combustion of coal, petroleum, biofuel and biomass (55 combustion fuel types, defined in Wang et al., 2013). In contrast to previous studies (Luo et al., 2008; Ito, 2013), the emission of Fe was calculated based on the Fe content in each type of fuel, the partitioning of Fe between residue ash, cyclone ash and fly ash, the size distribution of Fe-contained particles, and the efficiency of removal by different types of control device. A similar method has been recently applied to estimate the emissions of phosphorus from combustion sources (Wang et al., 2015). Only the fly ash is emitted to the atmosphere but other types of ashes are not. For a specific combustion fuel type, the emission (E) can be calculated as:

$$E = a \cdot b \cdot c \cdot (1-f) \cdot \sum_{x=1} J_x \cdot \left[\sum_{y=1}^{4} A_y \cdot (1-R_{x,y}) \right] \quad (1)$$

where x is a given particle size discretized into n bins (two bins for petroleum and three bins for coal and biomass), y is a specific control device (cyclone, scrubber, electrostatic precipitator, or no control), a is the consumption of fuel, b is the completeness of combustion (defined as the fraction of fuel burnt in the fires), c is the Fe content of the fuel, f is the fraction of Fe retained in residue ash relative to the amount of Fe in burnt fuel, J_x is the fraction of Fe emitted in particle size x, A_y is the fraction of a specific control device, and $R_{x,y}$ is the removal efficiency of control device y for particle size x. For all parameters in equation (1), the values or ranges are listed in **Table 1** and briefly described as below. The Fe in coal fly ash was divided into three size bins: 0.1-0.3% in PM_1 (diameter <1 μm), 10-30% in PM_{1-10} (diameter 1-10 μm), and the remainder in $PM_{>10}$ (diameter >10 μm) (Querol et al., 1995; Yi et al., 2008). The Fe in biomass fly ash was also divided into three size bins: 1-3% in PM_1, 50-60% in PM_{1-10}, and the remainder in $PM_{>10}$ (Latva-Somppi et al., 1998; Valmari et al., 1999). The Fe in oil fly ash was divided into two size bins: 80-95% in PM_1 and the remainder in PM_{1-10} (Mamane et al., 1986; Kittelson et al., 1998). Fuel consumption data are distributed spatially at a 0.1° × 0.1° resolution in PKU-FUEL-2007 (Wang et al., 2013), established for year 2007, combined with country data to obtain temporal changes from 1960 to 2006 (Chen et al., 2014; Wang et al., 2014a). Fixed completeness of combustion (b) were assigned to coal (98%), petroleum (98%), wood in stoves (88%), wood in fireplaces (79%) and crop residues (92%) (Johnson et al., 2008; Lee et al., 2005; Zhang, et al. 2008). As the fuel consumptions for biomass burning have already accounted for the completeness of combustion based on the type of fires (van der Werf et al., 2011), we applied a combustion completeness of 100% for them. The percentage of each control device (A_y) was calculated by year and country in our previous studies (Chen et al., 2013; Wang et al., 2014a,b) using a method based on S-shaped curves (Grubler et al., 1999; Bond et al., 2007).

2.2 Fe contents in fuel

Fe contents in coal were derived for 45 major coal-producing countries, such as China, US, Russia, India, Indonesia and Australia, from the World Coal Quality Inventory (Tewalt et al., 2010), which is based upon 1379 measured data in each country. The collected Fe content in coal followed log-normal distributions (**Fig. S1**), and the means and standard deviations (σ) of $\log_{10}$-transformed Fe contents in coal were derived for each country (**Table S1**). Fe content of coal burned in each country was then calculated including imported coal using the coal-trading matrix among countries (Chen et al., 2014). The variation of Fe content among different coal types (which differs by 20% between bituminous coal and lignite produced in Turkey as an example) is smaller than that of coal produced in different countries and thus ignored in our study. In addition to coal, Fe contents of wood, grass, and crop residues were taken from a review study (Vassilev et al., 2010), also following log-normal distributions (**Fig. S1**). The means and σ of the $\log_{10}$-transformed Fe contents were thereby derived for wood, grass, and crop residues separately. We applied the Fe content in grass (-3.57±0.34 for $\log_{10}$-transformed Fe content) for the savanna and grassland fires and the Fe content in wood (-3.45±0.57) for the deforestation, forest, woodland and peat fires. In addition, the means and σ of Fe contents were 0.13±0.09 % for dung cakes (Sager et al., 2007) and 0.00024±0.00023 % for biodiesel (Chaves et al., 2011), 32±2 ppm for fuel oil (Bettinelli et al., 1995), 13±7 ppm for diesel, 3.3±2.6 ppm for gasoline, and 4.9±3.3 ppm for liquefied petroleum gas (Kim et al., 2013).

2.3 Partitioning of Fe in combustion

The fraction of Fe retained in residue ash (*f* in **Eq 1**) during coal combustion has been measured for few real-world facilities: 43-45% in a power plant in India (Reddy et al., 2005), 30% in a power plant equipped with a bag-house in China (Yi et al., 2008), 40% in a fluidized bed boiler (Font et al., 2012), and 30-40% (measured for Mn, which is similar to Fe) in two power plants in China (Tang et al., 2013). We therefore applied a percentage of 30-45% for Fe retained in residue ash during the combustion of coal in industry and power plants. For the combustion of petroleum, 43% and 58% of the Fe in petroleum in a small-fire-tube boiler and a combustor representative for a larger utility boiler, respectively, were emitted in fly ash (Linak et al., 2000). A range of 43-58% was thus adopted for Fe emitted into fly ash for petroleum burned in power plants and industry. For solid biofuels burned in industry, 60-70% of the Fe was retained in the residue ash (Ingerslev et al., 2011; Narodoslawsky et al., 1996), which was the range adopted in this study.

The budget of Fe from the combustion of petroleum by motor vehicles has received little attention, likely due to the low Fe content in petroleum. Wang *et al.* (2003) reported that 93% Fe in petroleum was released into the atmosphere, and thus we applied a percentage of 93±5% for Fe emitted into the atmosphere.

The partitioning of Fe from the combustion of various fuels in residential sector has not been studied. The concentrations of Fe in residue ash and fly ash are similar (Meji, 1994), so the fraction of Fe emitted into the atmosphere was derived from the ratio of the mass of Fe in fly ash to that in the fuel. We thereby derived the fraction of Fe retained in residue ash (*f* in **Eq 1**) from the burning of anthracite coal (99.6±0.4%) (Chen et al., 2006; Shen et al., 2010), bituminous coal (94±3%) (Chen et al., 2006; Shen et al., 2010), crop residues (87±8%) (Li et al., 2007), and wood (94±5%) (Shen et al., 2012) burned in residential stoves or fireplaces.

Many studies measured the budget of elements other than Fe in the open burning of biomass. We collected the budget measured for elements whose physical and chemical properties are similar to those for Fe (*e.g.* low volatility). In the literature, the percentage of the element transfer to the atmosphere based on the

element present in initial fuels was converted to that based on that in burnt fuels using the completeness of combustion (Raison et al., 1985; Pivello and Coutinho, 1992; Mackensen et al., 1996; Holscher et al., 1997). Many studies measured the budget of elements other than Fe in the burning of biomass. We collected the budget measured for elements whose physical and chemical properties are similar to those for Fe (e.g. low volatility). In the literature, the percentage of the element transfer to the atmosphere based on the element present in initial fuels was converted to that based on that in burnt fuels using the completeness of combustion (Raison et al., 1985; Pivello and Coutinho, 1992; Mackensen et al., 1996; Holscher et al., 1997). Raison et al. (1985) reported that 44-59% of the manganese in burnt fuel was transferred to the atmosphere in three prescribed vegetation fires (f = 41-56%). Pivello and Coutinho (1992) reported that 63% of the potassium, 76% of the calcium and 61% of the magnesium in burnt fuel were transferred to the atmosphere in a Brazilian savanna fire (f = 24-39%). Mackensen et al. (1996) reported that 18-51% of the potassium in burnt fuel was transferred to the atmosphere for two plots of forest fires in eastern Amazonia (f = 49-82%). Holscher et al. (1997) reported that 50% of the calcium and 57% of the magnesium in burnt fuel was transferred to the atmosphere during a deforestation fire in Brazil (f = 43-50%). Laclau et al. (2002) reported that 61% of the potassium, 79% of the calcium and 72% of the magnesium were bound in residue ash in the complete combustion of leaf litter from the littoral savannas of Congo (f = 61-79%). Chalot et al. (2012) reported that 70% of the copper and 55% of the zinc in all combustion products were bound in residue ash in the combustion of phytoremediated wood (f = 55-70%). In summary, we assumed that the partitioning of Fe is similar to these analogue elements, and applied a fraction of Fe in residue ash in burnt fuel (f) of 49-82% for forest fires (Mackensen et al., 1996; Chalot et al., 2012), 24-79% for savanna fires (Pivello and Coutinho,1992; Laclau et al., 2002), 43-50% for deforestation (Holscher et al., 1997), and 41-56% for woodland and peat fires (Raison et al., 1985). Here, the percentage of Fe transferred to the atmosphere for biomass burning in the field is larger than that in the residential stoves (see values above) and this is likely due to the wind which can uplift more combustion ashes into the air in the case of wildfires (Pivello and Coutinho, 1992).

2.4 Spatial allocation of Fe emissions from combustion

Iron emissions from combustion sources were allocated to 0.1° × 0.1° grids for 2007 and to 0.5° × 0.5° grids for 1960-2006. The annual emissions of Fe were estimated based on the 0.1° gridded fuel data which is used to construct a global CO_2 emission inventory (Wang et al., 2013; available at http://inventory.pku.edu.cn/home.html) and on country-specific parameters for 2007. For other years, Fe emissions from fossil fuels and biofuel were first calculated at the national level and then allocated to 0.5° grids by sector (energy, residential, transportation, and industry) using the emission distribution of black carbon (BC) in each year for the same sector from the MACCity inventory (Lamarque et al., 2010; Granier et al., 2013) as a proxy. Gridded emissions from wildfires were estimated from carbon emission data at a resolution of 0.5° × 0.5° compiled by GFED3 (Global Fire Emissions Database version 3) (van der Werf et al., 2010) for 1997-2007 and by RETRO (REanalysis of the TROpospheric chemical composition over the past 40 years) for 1960-1996 (Schulz et al., 2008). RETRO does not provide data for deforestation fires separately, so that the average fractions of deforestation fires in total forest fires by GFED3 were applied for 1960-1996.

2.5 Uncertainty of Fe emissions from combustion

A Monte Carlo ensemble simulation was run 1000 times by randomly varying parameters in the model, including fuel consumption, the Fe content, the fraction of Fe retained in the residue ash, the size distribution of Fe emission and the technology division of control device. Normal (petroleum, biodiesel, and dung cake) or log-normal (coal, grass, wood, and crop residues) distribution was adopted for the Fe content of fuel, as described above. The fraction of Fe retained in the residual ash was assumed to be uniformly distributed with ranges summarized in **Section 2.3**. Uncertainties in the fuel-consumption data and the technology divisions were quantified by prescribing a uniform distribution with a fixed relative standard deviation, as introduced in the previous studies (Wang et al., 2013; Chen et al., 2013; Wang et al., 2014a).

2.6 Emissions of Fe from mineral sources

We estimated the content of Fe in dust based on the largest mineralogical database to date (Journet et al., 2014). Journet et al. (2014) provided global 0.5° × 0.5° maps for six types of Fe-containing minerals (illite, smectite, kaolinite, chlorite, vermiculite, and feldspars) and two types of Fe oxides (hematite and goethite) in the clay (<2.0 μm) and only goethite in the silt (>2.0 μm) fraction. Then, a global 0.5° × 0.5° map of Fe content in clay fraction was obtained (**Fig. S2**) with the Fe content of each mineral (4.3% for illite, 2.6% for smectite, 0.23% for kaolinite, 12.5% for chlorite, 6.7% for vermiculite, 0.34% for feldspars, 62.8% for goethite and 69.9% for hematite) measured in Journet et al. (2008) and compiled in Journet et al. (2013). Note that we only account for the variation of dust emissions when assessing the uncertainty in Fe emissions from dust. However, there is also a variation of elemental composition of minerals in nature. For example, the Fe content can vary from 0.8 to 8.4% in illite depending on the environmental condition (Murad and Wagner, 1994), and from 0.02 to 0.81% in kaolinite (Mestdagh et al., 1980). This uncertainty is not accounted for in our study due to lack of a global distribution of elemental composition in minerals. At last, the LMDz-INCA global model (**Section 2.7**) was run for 2000-2011 at a resolution of 0.94° latitude by 1.28° longitude to produce an averaged field of dust emissions.

2.7 Modelling the atmospheric transport and deposition of Fe aerosols

We used the LMDz-INCA global chemistry-aerosol-climate model coupling on-line the LMDz (Laboratoire de Météorologie Dynamique, version 4) General Circulation Model (Hourdin et al., 2006) and the INCA (INteraction with Chemistry and Aerosols, version 4) model (Hauglustaine et al., 2004; Schulz, 2007; Balkanski, 2011) to simulate the atmospheric transport and distributions of Fe emitted from combustion and mineral sources. The interaction between the atmosphere and the land surface is ensured through the coupling of LMDz with the ORCHIDEE (ORganizing Carbon and Hydrology In Dynamic Ecosystems, version 9) dynamical vegetation model (Krinner et al., 2005). In the present configuration, the model was run at a horizontal resolution of 0.94° latitude by 1.28° longitude with 39 vertical layers from the surface to 80 km. In all simulations, meteorological data from the European Centre for Medium-Range Weather Forecasts (ECMWF) reanalysis have been used. The relaxation of the GCM winds towards ECMWF meteorology was performed by applying at each time step a correction term to the GCM predicted u and v wind components with a relaxation time of 6 h (Hourdin and Issartel, 2000; Hauglustaine et al., 2004). The ECMWF fields are provided every 6 hours and interpolated onto the LMDz grids.

In the model, the emissions of dust were calculated as a function of wind velocities at a height of 10 m (with a threshold value) and of the clay content from dust source locations (Schulz et al., 1998; Balkanski et al., 2007). The simulated concentrations and optical depths of dust have been validated by measurements (Schulz

et al., 1998; Guelle et al., 2000; Balkanski et al., 2004, 2007). For transport, the model uses a computationally efficient scheme to represent the size distribution of dust. The tracer is treated as a log-normal distribution with a mass median diameter (MMD) and a fixed geometric σ (defined as the σ of log-transformed sizes). Hygroscopic growth and removal processes are assumed to affect the MMD rather than the width of the distribution (Schulz et al., 1998, 2007). After being emitted, dust with a MMD of 2.5 μm and a geometric σ of 2.0 is transported and removed by sedimentation (Slinn and Slinn, 1980), wet and dry deposition (Balkanski et al., 2004, 2010, 2011).

The emitted Fe from combustion sources were partitioned into three particulate modes with the following characteristics: Fe in PM_1 as a fine mode (MMD = 0.34 μm, geometric σ = 1.59); Fe in $PM_{1\text{-}10}$ as a coarse mode (MMD = 3.4 μm, geometric σ = 2.0); Fe in $PM_{>10}$ as a super coarse mode (MMD = 34.0 μm, geometric σ = 2.0) (Mamane et al., 1986; Querol et al., 1995; Valmari et al., 1999). Hygroscopic growth, sedimentation, dry and wet deposition accounted for Fe in $PM_{1\text{-}10}$ and $PM_{>10}$, as for dust, and Fe in PM_1 as for BC (Balkanski et al., 2004, 2010, 2011). Hygroscopic growth of particles in the model is treated as a function of ambient relative humidity and the composition of soluble aerosol components based on Gerber's experiment work (Gerber, 1988). The uptake of water on aerosols increases the particle size of Fe, while the loss of water on aerosols decreases the particle size of Fe. For the particle density, the fraction of low density mass in coal fly ash is found to increase with decreasing particle size (Furuya et al., 1987). The major fraction for particles with a diameter less than 10 μm is composed by mass with a density of 2.4-2.8 g cm^{-3}, and by mass with a density of 1.6-2.4 g cm^{-3} for particles with a diameter from 10 to 100 μm. Therefore, we applied a density of 2.6 and 2.0 g cm^{-3} for Fe transported in $PM_{1\text{-}10}$ and $PM_{>10}$ respectively in the model. For Fe in PM_1, we assumed that the density is the same as BC (1.5 g cm^{-3}). For the hygroscopic properties of Fe, it is found that Fe in large-size coal ash is dominated in aluminosilicate glass, similar to that in dust (Chen et al., 2012), and thus we assume that the Fe in $PM_{1\text{-}10}$ and $PM_{>10}$ can be treated as insoluble dust, which is removed by sedimentation, dry deposition and below-cloud scavenging. For the Fe in PM_1, it is found that approximately 25% of Fe in fine particle (diameter<0.61 μm) is bound to organic matter and thus insoluble (Espinosa et al., 2002). Thus, we assumed that 25% of Fe in PM_1 was hydrophobic, which is removed by sedimentation, dry deposition and below-cloud scavenging, but not by in-cloud scavenging. The remainder Fe in PM_1 was hydrophilic, which is removed by sedimentation, dry deposition, below-cloud scavenging, and in-cloud scavenging. Due to limited understanding of the heterogeneous chemistry of Fe in the cloud, we did not account for the conversion of Fe from hydrophobic to hydrophilic in the atmospheric transport, and the ratio between the two phases varies due to their different removal rates in the atmosphere.

Running the model for the whole period 1990-2007 was too heavy computational. Therefore, we run the model for one representative year. We plan to run the simulations for more years for a future study. In the present study, simulations were run for a typical year (2005) for the Fe emitted from the combustion of coal (three size classes), petroleum (two size classes) and biomass (three size classes). The Fe emitted from combustion as monthly means averaged over 1990-2007 were used as an input to the model, which produces the distribution of Fe concentrations attached to aerosols in the surface layer of the atmosphere contributed by combustion sources. When evaluating the modelled Fe concentrations by observations, we added the Fe concentrations contributed by combustion sources and dust together. However, there is a notable temporal variation of the combustion-related emissions over this period. The coefficient of variation (defined as the

standard deviation relative to the mean) of annual Fe emissions from combustion over 1990-2007 is 46, 28, 17, 22, 26 and 22% for Europe, North America, South America, Africa, Asia and Oceania, respectively. To account for the impact of the changing emissions, when comparing the model with observations, we scaled the modelled Fe concentration from combustion at each land site by the ratio of the national Fe emission in the year to the 1990-2007 average in the country, and then compare it with the measured concentrations. For sites in the oceans, we scaled the concentrations following the same method using the global total emissions. In addition, since the change of land use during the period has not been accounted for when estimating the dust emissions in the model, we used the average Fe concentration by dust over 2000-2011 when comparing against observations and estimating the average contribution to Fe concentrations by different sources. Therefore, uncertainties induced by the nonlinearity of Fe concentrations to emissions and the interannual variation of dust emissions have not been accounted for in our study, which should be notified when comparing the model against the observations

3 Emission sources of Fe

3.1 Emissions of Fe from combustion

Based on the fuel consumptions and Fe emission rates, the average global Fe emissions for 1960-2007 was 5.3 Tg yr^{-1} from combustion sources, with 0.046, 1.4, and 3.8 Tg yr^{-1} of Fe emitted in PM_1, $PM_{1\text{-}10}$, and $PM_{>10}$, respectively. The Monte Carlo simulation of emission parameters shows that the Fe emissions were log-normally distributed (**Fig. 1**). The σ of $\log_{10}$-transformed Fe emissions ($\log_{10}\sigma$) was 0.22 for the global total, corresponding to a 90% confidence range of 2.3 to 12.1 Tg yr^{-1}, or -56% to +128% relative to the central estimate. In addition, the $\log_{10}\sigma$ varied from 0.09 (petroleum) to 0.27 (coal) for the emissions from different fuels (**Fig. 1A**). Due to a relatively large error in the Fe content of coal, the range of uncertainty of Fe emission from coal was larger than that of other fuels. Removing the variations of Fe content in fuel reduced the overall variation ($\log_{10}\sigma$) of Fe emissions by 66% (coal), 34% (petroleum) and 50% (biomass). Consequently, a large contribution of uncertain Fe content in coal causes the range of uncertainty of Fe emissions in coarse particles to be larger than in fine particles (**Fig. 1B**). The uncertainty ranges in the estimated emissions from fossil fuels and biomass for selected years are listed in **Table 2**.

The relative contributions of combustion sources to Fe emissions in different sizes are shown in **Fig. 2**. It shows that Fe emissions in medium-to-coarse particles ($PM_{1\text{-}10}$ or $PM_{>10}$) are dominated by the combustion of coal in power plants and industry, followed by a notable contribution from the natural burning of biomass. By contrast, the combustion of petroleum (32%), followed by coal (34%) and biomass (34%), contributed most to Fe emissions in fine particles (PM_1). The different source profiles are important for determining the Fe solubility and are discussed in **Section 7**. For example, the observed solubility of Fe might be primarily controlled by the particle size of dust (Baker and Jickells, 2006), but also varies in the fly ash from different fuels (Schroth et al., 2009; Bowie et al., 2009; Chen et al., 2012).

3.2 Spatial distributions of Fe emissions from combustion sources

Fe emissions for 2007 from combustion in fine (PM_1) and medium-to-coarse ($PM_{1\text{-}10}$ and $PM_{>10}$) particles are shown in **Fig. 3**. The spatial patterns were similar between Fe emitted in fine and medium-to-coarse particles, with high emission density in the populated regions of East Asia and South Asia, the industrialized regions of Europe and North America, and the frequently burned forests and savannas of South America and Africa.

Some patterns, however, also differed between them regionally. For example, the Fe emission density of medium-to-coarse particles was much higher in Asia than in western Europe and eastern North America. By contrast, the Fe emission density of fine particles has similar high values among these regions, due to a large contribution by the burning of petroleum in motor vehicles and power plants in Europe and North America, and to low removal efficiency for fine particles in industry (Yi et al., 2008). Particularly, there were notable high Fe emission density in fine particles in the northern Atlantic and northern Pacific Oceans from shipping, which can contribute to soluble Fe in the water through local deposition. The emission density of Fe in PM_1 is much lower than Fe in $PM_{1\text{-}10}$ and $PM_{>10}$, and but still important due to a higher solubility and longer lifetime in the transport (Baker and Jickells, 2006).

3.3 Temporal trends of Fe emissions from combustion sources

The temporal changes of Fe emissions from combustion sources for 1960-2007 were derived for fine (PM_1) and medium-to-coarse ($PM_{1\text{-}10}$ and $PM_{>10}$) particles (**Fig. 4**). Changes in both fuel consumption and control devices together control the temporal trends. For example, Fe emissions of both fine and medium-to-coarse particles had decreased since 1990 in Europe due to the switch from coal to gas and other sources of energy (*i.e.* solar and nuclear energy) (International Energy Agency, 2008), and also to policy regulations to implement emission control facilities (Vestreng et al., 2007). Similarly, the replacement of residential coal by petroleum or natural gas, and the implementation of policies enforcing control facilities around 1990 in China (Ministry of Environmental Protection of the People's Republic of China, 2008) together led to a slowdown or even a reversal of the increase of Fe emissions in the region.

The temporal trends of Fe emissions of fine and medium-to-coarse particles also notably differed. Before 1985, Fe emissions of fine and medium-to-coarse particles both increased, due to a rapid increase in fuel consumptions. After 1985, Fe emissions of fine particles first decreased and re-increased after 2000, while Fe emissions of medium-to-coarse particles continuously decreased. Two explanations can account for the decoupling. First, the control devices equipped in industry can remove Fe in medium-to-coarse particles more effectively than fine particles (Yi et al., 2008). Second, the consumption of petroleum has been increasing in both developed and developing countries, sustaining fine-particle Fe emissions. In particular, Fe emission in fine particles in Asia had increased recently after a respite in the 1990s. The spatial distributions of Fe emissions from combustion sources from 1960 to 2007 are shown in **Fig. S3**. The emission centers have shifted from Europe and North America to Asia over the past five decades, in agreement with the trends shown in **Fig. 4**.

3.4 Mineral sources of Fe

Based on the soil mineralogical data (Journet et al., 2014), the estimated global total emission of Fe from mineral sources ranged from 34.4 to 54.2 Tg yr^{-1} for 2000-2011, with an average emission of 41.0 Tg yr^{-1}. The modelled average global total emission of dust for 2000-2011 was 1040 Tg yr^{-1}, close to the median of 14 AeroCom Phase I models (1120 Tg yr^{-1}) (Huneeus et al., 2011). Our estimated Fe emission from dust is lower than the 55-74 Tg yr^{-1} reported by Luo et al., 2008 and Ito, 2013, mainly because the emission of dust is larger in the models used by these authors. For example, the model used by Luo et al., 2008 simulated a total dust emission of 4313 Tg yr^{-1} higher than other 13 AeroCom Phase I models (Huneeus et al., 2011), including LMDz-INCA. However, the dust emission is very size-dependent, and the emissions should be evaluated by prescribing the size distribution in source regions to the transport models.

The average Fe emission density from mineral sources for 2000-2011 is mapped in **Fig. 5A**. The major source regions include the Sahara Desert, southern Africa, Middle East, northwestern China, southwestern North America, southern South America, and western Australia. The estimated Fe emission map based on the new soil mineralogical data set (Journet et al., 2014) is also compared to that derived using a constant Fe content (3.5%) (**Fig. 5B**) as measured by Taylor and McLennan (1985) and widely used in other models (Luo et al., 2008; Mahowald et al., 2009; Ito, 2013). The new mineralogical data set led to a larger Fe emission density over the Sahara, Arabian, and Takla-Makan Deserts, and a lower Fe emission density over the Gobi Desert, reflecting the difference of Fe content of dust relative to 3.5% (**Fig. S2**).

3.5 Comparison of Fe emissions with previous studies

Table 2 summarizes the comparison of our estimations of Fe emissions with previous studies (Bertine and Goldberg, 1971; Luo et al., 2008; Ito, 2013). Bertine and Goldberg (1971) estimated the emissions of fifty-one trace elements into the atmosphere from fossil fuel combustion (1.4 Tg yr^{-1} for 1967) based on a mass-balance method similar to ours. However, due to a lack of measurement data at the time, they assumed that 10% of all trace elements in fuels was transferred to the atmosphere. This rate is lower than the 30-45% measured for Fe in recent studies (Yi et al., 2008; Font et al., 2012; Tang et al., 2013). The estimate by Bertine and Goldberg (1971) for the same year (1967) is within the uncertainty range of our estimate (1.2-7.2 Tg yr^{-1} as 90% confidence), but half of our central estimate (3.0 Tg yr^{-1}) after accounting for different removal efficiencies by particle size and control device.

Luo et al. (2008) and Ito (2013) have estimated Fe emissions from the combustion of fossil fuels, biofuels and biomass burning in fine (PM_1) and medium particles (PM_{1-10}). Their estimates of the total Fe emissions (1.7 Tg yr^{-1} for 1996 and 2001) are close to our central estimates (1.6 Tg yr^{-1} for 1996 and 1.3 Tg yr^{-1} for 2001 with a 90% confidence range of 0.7-3.8 and 0.6-3.1, respectively). For fossil fuels, Luo *et al.* (2008) and Ito (2013) estimated Fe emissions based on the particle emission factors and the Fe contents of particles. Their estimates of fossil fuel emissions (0.51 Tg yr^{-1} for 1996 to 0.66 Tg yr^{-1} for 2001) are close to the lower bound in the uncertainty range of our estimates (0.6-2.5 Tg yr^{-1} as 90% confidence for 1996 and 0.4-1.8 Tg yr^{-1} for 2001) and lower than our central estimates (1.2 and 0.9 Tg yr^{-1} for the two years, respectively) for the same size class (**Table 2**). In the method used by Luo *et al.* (2008) and Ito (2013), the Fe contents of particles are measured in very few studies. For example, for coal burnt in power plants and industry, there are only three measurements in the U.S.A. which were used by Luo *et al.* (2008), reporting an Fe content of 4.5-7.6% in fine particles and 8.1-9.4% in coarse particles (Olmez et al., 1988; Smith et al., 1979; Mamane et al., 1986). In addition to large uncertainty in sample collection (Hildemann et al., 1989), the variation of Fe content in particles is large. The measured Fe content in coal fly ash generated by the combustion of bituminous coal in Shanxi Province, China is 10.2-11.9% (Fu et al., 2012), 40% higher than the values used by Luo *et al.* (2008) and Ito (2013). A larger Fe content than that used by Luo *et al.* (2008) and Ito (2013) was also found for oil / biofuel fly ashes in the measurement by Fu et al. (2012). The large variation of Fe content of particles explains part of the underestimation in the estimates by Luo *et al.* (2008) and Ito (2013). In addition, Luo *et al.* (2008) and Ito (2013) estimated that the Fe emission ratio between PM_1 and PM_{1-10} is 1:6, compared to 1:24 in this study. The emission ratios used by Luo et al. (2008) and Ito (2013) were taken from Bond et al. (2004), which pertained to carbonaceous matter in fine particles but was not justified for Fe (mainly in coarse particles). For biomass burning, our central estimates of the total Fe emissions are lower

than that by Luo et al. (2008) and Ito (2013). Luo et al. (2008) applied a globally constant Fe:BC emission ratio based on the slope of Fe and BC concentrations observed for aerosols in the Amazon Basin. Note that the dust and plant material entrained in fires can contribute to the Fe concentrations in the atmosphere, as noticed by Luo et al. (2008). As a result, their estimates include the pyro-convection of Fe from soils and plant materials. In contrast, our estimate is based on the mass balance of Fe from the burnt fuels. This might explain partly why our estimate of the biomass burning emissions of Fe is lower than that in previous studies (Luo et al., 2008; Ito, 2013). Although our estimate provides an explicit source attribution of Fe, which is useful for modelling the Fe solubility, it underestimates the total sources. We propose that the emissions of Fe by pyro-convection in the fires should be estimated separately in the future.

In a recent study focused on East Asia (Lin et al., 2015), the emission of Fe from combustion sources in East Asia in 2007 was estimated to be 7.2 Tg yr^{-1}, far higher than all other studies (Luo et al., 2008; Ito, 2013) and the central estimate in our study (1.6 Tg yr^{-1}, with a 90% confidence of 0.66-3.84). The authors used an alternative method to estimate the emission of Fe based upon the sulfur dioxides (SO_2) emission and the ratio of sulfur and Fe content in fuels. As pointed out by the authors, the emission of Fe from iron and steel industries is likely to be more important than previously thought. However, the authors also pointed out a notable uncertainty in their estimate because some parameters (e.g, the ratio of bottom ash to fly ash) are very uncertain due to the lack of measurements (Lin et al., 2015). The value taken for the ratio of bottom ash to fly ash in that study is from a single measurement that took place in Taiwan (Yen, 2011). Due to the lack of a sufficient number of measurements for some parameters, our method cannot be applied to estimate the global Fe emission from the individual sector of iron and steel industries. These remarks show that measurements are urgently needed to constrain the iron content of aerosols emitted from the iron and steel industries as well as other sectors.

4 Modelling of Fe concentrations

4.1 Spatial distribution of Fe concentrations in surface air

Based on the emissions of Fe from combustion sources as an average for 1990-2007 and mineral sources as an average for 2000-2011, the global distribution of annual mean Fe concentrations attached to aerosols in surface air was derived (**Fig. 6**).

Globally, Fe emissions were much higher from mineral sources (41.0 Tg yr^{-1}) than from combustion sources (5.3 Tg yr^{-1}). The modelled spatial distribution of Fe concentrations in surface air was thus dominated by mineral sources, in agreement with previous studies (Luo et al., 2008; Mahowald et al., 2009; Ito, 2013). Large Fe concentrations (>1.0 μg m^{-3}) are simulated over northwestern Africa, southwestern North America, western China, the Middle East, southwestern Africa and central to northern Australia. In addition to these continent regions, large Fe concentrations (>0.1 μg m^{-3}) are found over a large region of the Atlantic Ocean from 0 to 30°N due to the outflow of dust from the Sahara Desert, and large Fe concentrations (>0.5 μg m^{-3}) are found over the Arabian Sea and the Indian Ocean due to the outflow of dust from the Arabian, Lut and Thar Deserts.

4.2 Evaluation of Fe concentrations in surface air

The Fe concentrations attached to aerosols in surface air simulated for pixels of 0.94° latitude by 1.28° longitude were evaluated by 529 measurements obtained between 1990 to 2007. These measurements include

data compiled by Mahowald et al. (2009) and Sholkovitz et al. (2012) and our collation of data from peer reviewed studies (**Table S2**). The modelled Fe concentrations attached to aerosols in surface air, averaged for the months in the year of measurements, are plotted against the measured concentrations after scaling the Fe concentrations from combustion sources (**Section 2.7**) (**Fig. 7A**). The simulated Fe concentrations were grouped into same size range as measurements if the size was specified in the measurements and otherwise they were computed as total concentrations. The modelled spatial pattern matched the observations (r^2=0.53). Mahowald et al. (2009) compared modelled annual mean Fe concentrations to measurements. They pointed out that the daily measurements from cruises are not as representative as the long-term station measurements. Similarly, a better agreement can be achieved if all cruise measurements are excluded in the comparison (r^2 = 0.68) in our study (**Fig. 7B**).

Three statistical metrics were used to evaluate the model performance (**Table 3**): the fraction of stations with a deviation within a factor of two (F_2) or five (F_5) and the normalized mean bias (*NMB*). Globally, 57 and 78% of the stations were associated with deviations within factors of two and five, respectively, with an *NMB* of -14%. The model and observations agreed well for East Asia and the Atlantic Ocean, with deviations within a factor of two for 84 and 64% of stations, respectively. The model overestimated Fe concentrations at some stations over the Atlantic Ocean and the Mediterranean Sea. The model used only one major mode for dust (an initial MMD of 2.5 μm, and a fixed geometric σ = 2.0), which reproduces the long-range transport and dust optical thickness over the ocean (Schulz et al., 1998). Without more detailed size bins, we assumed that the Fe content of dust and the Fe content of soil in the clay fraction is the same. This assumption is a reasonable approximation for dust transported hundreds of kilometers away from the dust source regions (Formenti et al., 2014), because the lifetime of dust is much longer for the clay fraction (up to 13 days) than for the silt (4 to 40 hours) and sand (approximately 1 hour) fractions (Tegen and Fung, 1994). However, the mineralogy and therefore the density of material are not well considered in this simplification. This assumption would lead to an overestimation of the Fe content of dust near the source regions due to the ignored contribution of Fe in the silt and sand fractions (which have lower Fe contents than clay) (Formenti et al., 2014). To illustrate this impact, the global distribution of Fe content in dust simulated by assuming that Fe content of emitted dust is equal to that in the clay fraction of soil is shown in **Fig. S4**. We can see that the Fe content in dust over the Sahara Desert is 4.5-5.5%, which decreases with the distance to the Sahara Desert. According to a measurement at a site with a distance of about 2000 km to the Sahara Desert, the Fe content in dust is 2.5-2.7% when the dust is originated from local erosion and 4.3% when dust is originated from the Sahara Desert (Formenti et al., 2014). In the model, the Fe content is 4.5-5.5% over the Sahara Desert, which is higher than the measured 2.5-2.7%, and 4-5% over the regions distant from the Sahara Desert, close to the measured 4.3% in dust after a long-range transport from the Sahara Desert (Formenti et al., 2014). In addition, when compiling data in the mineralogy database, Journet et al. (2014) noticed that wet sieving is used to determine soil texture, leading to loss of soluble minerals (e.g., calcite or gypsum) and a possible overestimation of the content of minerals rich in Fe such as hematite and goethite. This impact might also contribute to an overestimation of Fe content in dust. The overestimation occurs mainly at stations near continents and the downwind of deserts in **Fig. 6**, indicating that the modelled Fe concentrations over the ocean were not excessively influenced. The model also underestimated Fe concentrations over the Pacific and Southern Oceans, likely due to the uncertainty in dust emissions and to the transport errors in the

Southern Hemisphere, which was documented previously (Huneeus et al., 2011, Schulz et al., 2012). Dust emissions over regions of the Southern Hemisphere, such as southern South America and southeastern Africa, require additional investigations.

One should note that modelled monthly mean concentrations were compared to daily measurements at some sites (*e.g.* measured by cruises) due to a lack of detailed date information in measurements. It also caused some discrepancies between model and observations. As pointed out by Mahowald et al. (2009), some cruise measurements were sensitive to episodic dust events. Mahowald et al. (2009) compared the modelled annual mean Fe concentrations to daily measurements, leading to a potential deviation by a factor up to 10. We also expected such a bias in this study, even though we were comparing modelled monthly Fe concentrations to all measurements. To address this influence, we compared modelled daily Fe concentrations to those from some cruise measurements with detailed date information available (Baker et al., 2006; Chen and Siefert, 2004). As illustrated in **Fig. 8**, particularly in **Fig. 8A** and **B**, the variation of daily concentrations could be well captured by the model. These variations were attenuated when using modelled monthly mean Fe concentrations. This agreement lends support to the estimation of annual mean Fe concentrations and thus Fe deposition in our study.

4.3 Fe concentrations over the Atlantic Ocean

The modelled Fe concentrations attached to aerosols in air near the Atlantic Ocean were compared against 296 transect cruise measurements for 2003-2008 (Baker et al., 2013) (**Fig. 9**). The zonal distribution of Fe concentrations was generally captured by the model (r^2 = 0.50). However, the model overestimated the Fe concentrations in the band between 10 and 20°N, because Fe content of the clay fraction was extrapolated to all dust types, leading to an overestimation of Fe concentrations at locations near dust source regions (see the discussion above). In addition, the model underestimated Fe concentrations by a factor of two at stations in the band between 40 and 70°S, and this model-data misfit could be reduced when the modelled concentrations were scaled by a higher dust emission in a sensitivity test (**Fig. 9**), confirming the high degree of uncertainties in dust emissions and transport in the Southern Hemisphere.

The seasonality of modelled Fe concentrations at two long-term monitoring stations on the western margin of the Atlantic Ocean (Bermuda and Barbados) was compared to the observations, collected between 1988 to 1994 during the AEROCE program (Arimoto et al. 1992, 1995, 2003; Huang et al., 1999) and compiled by Sholkovitz et al. (2009). As shown in **Fig. 10**, the observed seasonal variations of Fe concentrations at these two stations were well represented by the model, with peaks in summer corresponding to dust storms in the Sahara Desert.

4.4 Role of the combustion sources

The estimated total emissions and the spatial distributions of Fe from combustion sources differed from those of previous studies (**Table 2** and **Fig. 3**). The contribution of combustion sources to the Fe concentrations attached to aerosols in surface air is shown in **Fig. 11**. Large contribution of combustion sources (>80%) is found in western Europe, southeastern and northeastern China, southern Africa, central South America and eastern and northern North America, in agreement with the spatial distribution of combustion emissions.

To evaluate our estimation of the combustion sources of Fe, we divided all stations used in **Section 4.2** into four groups based on the contribution to Fe concentrations by combustion sources. We plotted the modelled Fe concentrations with or without combustion sources against the observations (**Fig. 12**). The model can

capture the observed Fe concentrations at 53 stations with combustion contributions larger than 50% well, with an average deviation of a factor of 1.5. The spatial pattern of Fe concentrations at these 53 stations is also well captured (r^2 = 0.73), lending good support to our new estimation of Fe emissions from combustion sources. The scatter for stations with a smaller combustion contribution indicates a higher uncertainty in mineral sources of Fe than combustion sources.

Due to too heavy computational load, we modelled the Fe concentrations from combustion in a typical year using the average Fe emissions during 1990-2007, and compared them with measurements during 1990-2007 by scaling the modelled Fe concentrations from combustion to a specific year with the temporal change of emissions at each site (**Section 2.7**). To investigate the influence of this scaling process, we compared the modelled Fe concentrations without scaling among the four groups of sites (see results in **Fig. S5**). As a result, without this scaling, there is very minor change in the comparison between the modelled and observed Fe concentrations with r^2 change from 0.73 to 0.72. It indicates that the variation of Fe concentrations among the measuring sites is dominated by the spatial variation of Fe concentrations.

4.5 Effect of the new mineralogical database

Fig. 13 shows the difference in modelled Fe concentrations using the new mineralogical data (Journet et al., 2014) relative to that using a constant Fe content in dust (3.5%), as widely adopted (Luo et al., 2008; Ito, 2013). The new mineralogical data increased the global total Fe emission from mineral sources from 38.5 to 41.0 Tg yr^{-1}, with a relative difference ranging from -60 to +30% regionally (**Fig. 5**). Iron emissions were lower over the Takla-Makan and Gobi Deserts (**Fig. 5**), leading to lower Fe concentrations over East Asia and the downwind regions over the northern Pacific Ocean. In contrast, Fe emissions were higher over the Sahara Desert and the deserts in the Middle East, southern Africa and central Australia (**Fig. 5**), leading to higher Fe concentrations over the Atlantic and Southern Oceans.

The effect of the new mineralogical database on the model-observation comparison at all stations used in **Section 4.2** is shown in **Fig. 14**. All stations were divided into four groups based on the relative differences in **Fig. 13**. The influence was not very significant. There are 49 stations with a relative difference larger than 30%, where the model bias was reduced from 40 to 20%. The new mineralogical data also led to modest improvements in the comparison of modelled and observed Fe concentrations in surface air over the Atlantic Ocean at all stations used in **Fig. 9** of **Section 4.3**, with a slight improvement of the underestimation at latitudes between 40 and 70°S (**Fig. S6**). The limited improvement obtained using the state-of-the-art mineralogical database implied that other factors, such as the dust emission uncertainties and the transport errors, influenced the estimation of Fe from mineral sources. Further studies are needed to constrain the dust emissions in the Southern Hemisphere in the model (Tagliabue et al., 2009; Schulz et al., 2012). The new mineralogical data provided information on the chemical form of the Fe in dust (Journet et al., 2014), which will help the modelling of Fe solubility.

4.6 Size distributions of Fe-containing particles

The particle size of Fe-containing particles is an important factor controlling the lifetime and solubility of Fe (Baker and Jickells, 2006; Mahowald et al., 2009). In LMDZ-INCA, the size distribution of Fe-containing particles was treated as a log-normal distribution with a varied MMD and a fixed geometric σ. **Fig. 15** shows the spatial distribution of modelled wet MMD of Fe-containing particles in surface air from combustion and mineral sources. The global average wet MMD of Fe-containing particles is 2.6 μm. The figure also

illustrates that the Fe was mainly attached to coarse particles (>5.0 μm) in regions dominated by combustion sources, such as in East Asia, South Asia, Europe, eastern and northern North America, South America and southern Africa. By contrast, the wet MMD of Fe-containing particles is 2.2-2.4 μm over the deserts dominated by mineral sources, such as in northern Africa, western Asia and southeastern North America, slightly smaller than the initialized wet MMD for dust.

According to Schulz et al. (2007), after the particles containing Fe are emitted into the atmosphere, there are three major processes that change the size distribution in the model. First, formation of sulphate increases the aerosol mass in the accumulation mode and, since the particle number is kept constant, the aerosol diameter increases for Fe in PM_1. Second, removing processes such as sedimentation removes the larger particles more efficiently, shifting the mode diameter to a smaller one for Fe in PM_1, PM_{10} and $PM_{>10}$. At last, the hygroscopic growth creates instaneous changes in the size of particles as a function of ambient relative humidity (Schulz et al., 2007), and the uptake of water on aerosols increases the size, while the loss of water on aerosols decreases the size. Therefore, the change of the size of Fe is dependent on the relative importance of the mechanisms increasing / decreasing the size. For example, the size of Fe in PM_1 emitted from coal combustion increased from 0.3 μm to >2 μm after being transported away from the source regions, because the hygroscopic growth by uptake of water on aerosol particles are more important. In contrast, the size of Fe in $PM_{>10}$ emitted from coal combustion in East Asia decreases over the southern Pacific Ocean, because sedimentation is the dominating process. The size of Fe in $PM_{>10}$ from coal combustion would decrease from 33 μm in the source regions to <10 μm over the oceans.

There are limited measurements of size distributions of Fe-containing particles. Sun et al. (2004) measured the Fe concentrations in $PM_{2.5}$ and PM_{10} at three stations in Beijing. The mean ± σ of the $PM_{2.5}/PM_{10}$ ratios of Fe was 28.1±7.8%, compared to 33.5±1.6% in our simulation. Chen and Siefert (2004) measured the Fe concentrations in $PM_{2.5}$ and total suspended particles (TSP) over the North Atlantic Ocean. The mean ± σ of the $PM_{2.5}$/TSP ratios of Fe was 55.2±16.8%, compared to the 49.9±0.5% in our simulation.

5 Global Fe deposition

The distribution of annual mean Fe deposition is shown in **Fig. 16**. Similar to the distribution of annual mean Fe concentrations attached to aerosols in surface air (**Fig. 6**), the spatial distribution of Fe deposition was dominated by mineral sources. High Fe deposition rates over the oceans were found over the Arabian Sea and the Indian Ocean (>100 mg m^{-2} yr^{-1}), followed by the Atlantic Ocean (10-100 mg m^{-2} yr^{-1}) and the northern Pacific Ocean (5-30 mg m^{-2} yr^{-1}). Mahowald et al (2009) pointed out that directly measured Fe deposition rates are very limited. We compared the modelled Fe deposition with *in situ* measurements compiled by Mahowald et al (2009). The spatial pattern of measured Fe deposition can be generally represented by the model (r^2 = 0.88) (**Fig. S7**). The limited data, however, prevented us from evaluating the modelled deposition rates globally.

6 Global atmospheric Fe budget

The atmospheric Fe budgets from different emission sources are summarized in **Table 4**. The atmospheric lifetime of Fe is highly dependent on the particle size, the emission source and the meteorological conditions. For example, the atmospheric lifetime changes from 0.08 days for Fe of $PM_{>10}$ from biomass burning to 4.1

days of PM_{1-10} and 9.4 days of PM_1, because larger particles can be more efficiently removed by sedimentation than smaller ones. The atmospheric lifetime also differs for Fe from different emission sources. For example, the atmospheric lifetime of Fe of PM_1 emitted from biomass burning is twice that for Fe of PM_1 emitted from coal combustion. For the wet deposition only, the atmospheric lifetime of Fe of PM_1 emitted from biomass burning was 15.2 days, compared to 9.4 days for Fe of PM_1 emitted from coal combustion. Less precipitation and scavenging over the dryer African savanna, the major region of Fe emissions from biomass burning, can explain this difference. The atmospheric burden of Fe and the atmospheric deposition of Fe over the oceans are both dominated by mineral sources, due to a larger total emission source.

We estimate that the annual deposition of total Fe over global oceans is 8.4 Tg yr^{-1} over the studied period (1990-2007). Among the total Fe deposition over the oceans, 93.1, 5.4, 1.4 and 0.13% was originated from dust (7.82 Tg yr^{-1}), coal combustion (0.455 Tg yr^{-1}), biomass (0.122 Tg yr^{-1}) and oil combustion (0.011 Tg yr^{-1}). In a recent global study modelling the Fe solubility, Ito (2015) estimated a larger deposition of Fe from mineral dust (13 Tg yr^{-1}), biomass burning (0.14 Tg yr^{-1}) and oil combustion (0.02 Tg yr^{-1}), but a lower deposition of Fe from coal combustion (0.16 Tg yr^{-1}), mainly due to the difference in the estimation for the sources (**Table 2**).

7 Influence of different Fe solubilities from different sources

The form and chemical properties of Fe vary greatly among different sources, which determine the solubility and bioavailability of Fe (Boyd et al., 2000; Moore et al., 2004). Measured Fe solubility is 77-81% in oil fly ash (Schroth et al., 2009) against only 20-25% in coal fly ash (Chen et al., 2012), and approximately 18% in biomass fly ash (Bowie et al., 2009). Note that solubility of Fe from any combustion sources is much larger than the 0.44% in dust from the Sahara Desert (Sedwick et al., 2007). One of the key findings of this study is the identification of Fe emissions from combustion sources. As shown in **Fig. 17**, the contribution by the combustion of petroleum and coal to the total Fe deposition exceeds 1% and 3%, respectively, over many oceans such as the northern Atlantic and northern Pacific Oceans. Considering their relatively high Fe solubility, the contribution of combustion sources to soluble Fe supply for these oceanic ecosystems could be amplified by 1-2 orders of magnitude. The additional input of soluble Fe from combustion sources may lead to profound biological effects over the northern Pacific, northern Atlantic and Southern Oceans, where Fe is identified as the primary limiting nutrient for the growth of phytoplankton (Moore et al., 2013). As a preliminary study, we calculated the deposition of soluble Fe from different sources using constant Fe solubilities (0.44% for dust, 22.5% for coal fly ash, 79% for oil fly ash and 18% for biomass fly ash). **Figure 18** shows the relative contribution of combustion-related Fe emissions to total soluble Fe deposition over global oceans. With a larger Fe solubility, the effective contribution of combustion sources is larger despite their smaller mass contribution than dust over most oceanic regions. As illustrated in **Fig. 19**, consideration of Fe from combustion sources, with assumed constant Fe solubilities for different sources, can largely improve the modelled soluble Fe concentrations when comparing against observations at 176 sites over the Atlantic and Pacific oceans (Baker et al., 2007; Sedwick et al., 2007; Buck et al., 2006; Buck et al., 2010). Further improvement of the modelled soluble Fe concentrations requires an explicit modelling of the atmospheric processing of Fe emitted from mineral dust and combustion sources, which is beyond the target

of present study. The produced maps of Fe deposition from different fuel types and from different sizes will help simulate the chemical processing of Fe in the atmosphere.

According to our estimation, combustion-related sources contribute 79% to the total deposition of soluble Fe over the oceans. Note that this estimate is dependent on the Fe solubility prescribed for different sources, and the influences by chemical, physical or photochemical factors have not been considered in our estimate. As a result, the predicted contribution by combustion-related sources to soluble Fe deposition over global oceans is 5 factors higher than the 15% estimated in a recent study (Ito, 2015). In that work, Ito has explicitly modelled the dissolution of Fe in fly ash due to photochemical reactions with inorganic and organic acids in solution. It results in a global average Fe solubility of 2% for dust, 21% for biomass fly ash, 8% for coal fly ash, and 65% for oil fly ash, which differs from the measurements used in our estimate (Sedwick et al., 2007; Bowie et al., 2009; Schroth et al., 2009; Chen et al., 2012). However, as also pointed out by Ito (2015), there is a large uncertainty in the modelled Fe solubility due to large uncertainties associated with prescribed Fe solubility at emission, which is dependent on the condition of combustion sources (Ito, 2015). More measurements of Fe solubility at various sources and open oceans should be conducted to simulate and constrain the Fe solubility in the future work.

In addition, the study by Lin et al. (2015) predicted that 87% and 41% of the deposition of soluble Fe over the Northwestern Pacific Ocean could be attributed to combustion-related sources when prescribing a solubility of 40% and 4% for Fe in fly ash, respectively. Their upper estimate agrees well with our prediction that combustion-related sources would contribute 80-95% to soluble Fe deposition in this region (**Fig. 18**).

8 Summary and conclusion

We developed a new emission inventory of Fe from combustion sources using Fe contents of fuel and Fe partitioning during combustion, and estimated the emissions of Fe from mineral sources based on a new soil mineralogical database. We calculated the global total Fe emissions of 0.046, 1.4, and 3.8 Tg yr^{-1} in PM_1, PM_{1-10} and $PM_{>10}$ from combustion sources, respectively. Although the total Fe emissions are similar, the size distributions and the source profiles differ from those in previous studies, which substantially influenced the Fe solubility in aerosols.

We evaluated the estimated new emissions of Fe from combustion and mineral sources. We introduced the estimated Fe emissions in a global transport model running at a resolution of 0.94° latitude by 1.28° longitude. The modelled Fe concentrations attached to aerosols in surface air were compared with 825 measurements worldwide. The measured Fe concentrations were generally predicted by the model, including the spatial distributions of Fe concentrations in each region, the zonal distributions of Fe concentrations over the Atlantic Ocean, and the seasonality of Fe concentrations on the western margin of the Atlantic Ocean. Importantly, agreement was good at stations where the Fe concentrations were dominated by combustion sources, supporting our new estimations of Fe emissions from combustion sources. The new mineralogical data produced modest improvements but provided useful information on the chemical form of Fe. An underestimation of Fe concentrations over the oceans in the Southern Hemisphere, however, may confirm the high uncertainty in dust emissions, which deserves further study.

We estimated a total Fe deposition sink of 8.4 Tg yr^{-1} over global oceans, 7% of which originated from combustion sources. The modelled Fe deposition rates were confirmed by a limited number of *in situ*

measurements. Fe deposition rates over most oceanic regions, however, have not been widely measured. The combustion of coal, petroleum and biomass, all with a much higher Fe solubility than that in dust, contributed considerably to the deposition of Fe over the northern Atlantic and northern Pacific Oceans. We speculate that this large amount of additional input of soluble Fe may have had an impact on the oceanic carbon cycle and the global climate.

Acknowledgements

The authors thank Ether/ECCAD for distribution of emission data used in this study. R.W. was supported by the 'FABIO' project, a Marie Curie International Incoming Fellowship from the European Commission. This work was also supported by the European Research Council Synergy Grant IMBALANCE-P (ERC-SyG-2013-610028). The simulations in this work were performed using DSM-CCRT resources under the GENCI (Grand Equipement National de Calcul Intensif) computer time allocation (grant 2014-t2014012201).

References:

Arimoto, R., Duce, R. A., Savoie, D. L., and Prospero, J. M.: Trace-elements in aerosol-particles from Bermuda and Barbados - concentrations, sources and relationships to aerosol sulfate, J. Atmos. Chem., 14, 439–457, doi:10.1007/Bf00115250, 1992.

Arimoto, R., Duce, R. A., Ray, B. J., Ellis, W. G., Cullen, J. D., and Merrill, J. T.: Trace elements in the atmosphere over the North-Atlantic, J. Geophys. Res.-Atmos., 100, 1199–1213, doi:10.1029/94jd02618, 1995.

Arimoto, R., Duce, R. A., Ray, B. J., and Tomza, U.: Dry deposition of trace elements to the western North Atlantic, Global Biogeochem. Cy., 17, 1010, doi:10.1029/2001gb001406, 2003.

Baker, A. R. and Jickells, T. D.: Mineral particle size as a control on aerosol iron solubility, Geophys. Res. Lett., 33, L17608, doi:10.1029/2006gl026557, 2006.

Baker, A. R., Jickells, T. D., Witt, M., and Linge, K. L.: Trends in the solubility of iron, aluminium, manganese and phosphorus in aerosol collected over the Atlantic Ocean, Mar. Chem., 98, 43–58, doi:10.1016/j.marchem.2005.06.004, 2006.

Baker, A. R., Weston, K., Kelly, S. D., Voss, M., Streu, P. and Cape, J.N.: Dry and wet deposition of nutrients from the tropical Atlantic atmosphere: Links to primary productivity and nitrogen fixation, Deep-Sea Res. Pt. I, 54, 1704-1720, 2007.

Baker, A. R., Adams, C., Bell, T. G., Jickells, T. D., and Ganzeveld, L.: Estimation of atmospheric nutrient inputs to the Atlantic Ocean from 50◦ N to 50◦ S based on large-scale field sampling: iron and other dust-associated elements, Global Biogeochem. Cy., 27, 755–767, doi:10.1002/Gbc.20062, 2013.

Balkanski, Y.: L'Influence des Aérosols sur le Climat, Thèse d'Habilitation à Diriger des Recherches, Université de Versailles Saint-Quentin, Saint-Quentin-en-Yvelines, 2011.

Balkanski, Y., Schulz, M., Claquin, T., Moulin, C., and Ginoux, P.: Global emissions of mineral aerosol: formulation and validation using satellite imagery, in: Emissions of Atmospheric Trace Compounds, edited by: Granier, C., Artaxo, P., and Reeves, C., Advances in Global Change Research, Springer Netherlands, Dordrecht, the Netherlands, 239–267, 2004.

727 Balkanski, Y., Schulz, M., Claquin, T., and Guibert, S.: Reevaluation of Mineral aerosol radiative forcings
728 suggests a better agreement with satellite and AERONET data, Atmos. Chem. Phys., 7, 81–95,
729 doi:10.5194/acp-7-81-2007, 2007.
730 Balkanski, Y., Myhre, G., Gauss, M., Rädel, G., Highwood, E. J., and Shine, K. P.: Direct radiative effect of
731 aerosols emitted by transport: from road, shipping and aviation, Atmos. Chem. Phys., 10, 4477–4489,
732 doi:10.5194/acp-10-4477-2010, 2010.
733 Bertine, K. K. and Goldberg, E. D.: Fossil fuel combustion and the major sedimentary cycle, Science, 173,
734 233–235, doi:10.1126/science.173.3993.233, 1971.
735 Bettinelli, M., Spezia, S., Baroni, U., and Bizzarri, G.: Determination of trace-elements in fuel oils by
736 inductively-coupled plasma-mass spectrometry after acid mineralization of the sample in a microwave-oven,
737 J. Anal. Atom. Spectrom., 10, 555–560, doi:10.1039/Ja9951000555, 1995.
738 Bond, T. C., Streets, D. G., Yarber, K. F., Nelson, S. M., Woo, J. H., and Klimont, Z.: A technology-based
739 global inventory of black and organic carbon emissions from combustion, J. Geophys. Res.-Atmos., 109,
740 D14203, doi:10.1029/2003jd003697, 2004.
741 Bond, T. C., Bhardwaj, E., Dong, R., Jogani, R., Jung, S. K., Roden, C., Streets, D. G., and Trautmann, N.
742 M.: Historical emissions of black and organic carbon aerosol from energy-related combustion, 1850–2000,
743 Global Biogeochem. Cy., 21, GB2018, doi:10.1029/2006gb002840, 2007.
744 Bowie, A. R., Lannuzel, D., Remenyi, T. A., Wagener, T., Lam, P. J., Boyd, P. W., Guieu, C., Townsend, A.
745 T., and Trull, T. W.: Biogeochemical iron budgets of the Southern Ocean south of Australia: decoupling of
746 iron and nutrient cycles in the subantarctic zone by the summer-time supply, Global Biogeochem. Cy., 23,
747 GB4034, doi:10.1029/2009gb003500, 2009.
748 Boyd, P. W., Watson, A. J., Law, C. S., Abraham, E. R., Trull, T., Murdoch, R., Bakker, D. C. E., Bowie, A.
749 R., Buesseler, K. O., Chang, H., Charette, M., Croot, P., Downing, K., Frew, R., Gall, M., Hadfield, M., Hall,
750 J., Harvey, M., Jameson, G., LaRoche, J., Liddicoat, M., Ling, R., Maldonado, M. T., McKay, R. M., Nodder,
751 S., Pickmere, S., Pridmore, R., Rintoul, S., Safi, K., Sutton, P., Strzepek, R., Tanneberger, K., Turner, S.,
752 Waite, A., and Zeldis, J.: A mesoscale phytoplankton bloom in the polar Southern Ocean stimulated by iron
753 fertilization, Nature, 407, 695–702, doi:10.1038/35037500, 2000.
754 Buck, C. S., Landing, W. M., Resing, J. A., and Lebon, G.T.: Aerosol iron and aluminum solubility in the
755 northwest Pacific Ocean: Results from the 2002 IOC cruise, Geochem., Geophy., Geosy., 7, Q04M07,
756 doi:10.1029/2005GC000977, 2006.
757 Buck, C. S., Landing, W. M., Resing, J. A., and Measures, C. I.: The solubility and deposition of aerosol Fe
758 and other trace elements in the North Atlantic Ocean: Observations from the A16N CLIVAR/CO2 repeat
759 hydrography section, Mar. Chem., 120, 57-70, 2010.
760 Chalot, M., Blaudez, D., Rogaume, Y., Provent, A. S., and Pascual, C.: Fate of trace elements during the
761 combustion of phytoremediation wood, Environ. Sci. Technol., 46, 13361–13369, doi:10.1021/Es3017478,
762 2012.
763 Chaves, E. S., de Loos-Vollebregt, M. T. C., Curtius, A. J., and Vanhaecke, F.: Determination of trace
764 elements in biodiesel and vegetable oil by inductively coupled plasma optical emission spectrometry
765 following alcohol dilution, Spectrochim. Acta B, 66, 733–739, doi:10.1016/j.sab.2011.09.006, 2011.
766 Chen, H., Laskin, A., Baltrusaitis, J., Gorski, C. A., Scherer, M. M., and Grassian, V. H.: Coal fly ash as a

767 source of iron in atmospheric dust, Environ. Sci. Technol., 46, 2112–2120, doi:10.1021/Es204102f, 2012. 25
768 Chen, Y. and Siefert, R. L.: Seasonal and spatial distributions and dry deposition fluxes of atmospheric total
769 and labile iron over the tropical and subtropical North Atlantic Ocean, J. Geophys. Res.-Atmos., 109,
770 D09305, doi:10.1029/2003jd003958, 2004.
771 Chen, Y. J., Zhi, G. R., Feng, Y. L., Fu, J. M., Feng, J. L., Sheng, G. Y., and Simoneit, B. R. T.:
772 Measurements of emission factors for primary carbonaceous particles from residential raw-coal combustion
773 in China, Geophys. Res. Lett., 33, L20815, doi:10.1029/2006gl026966, 2006.
774 Chen, Y. L., Wang, R., Shen, H. Z., Li, W., Chen, H., Huang, Y., Zhang, Y. Y., Chen, Y. C., Su, S., Lin, N.,
775 Liu, J., Li, B. G., Wang, X. L., Liu, W. X., Coveney, R. M., and Tao, S.: Global mercury emissions from
776 combustion in light of international fuel trading, Environ. Sci. Technol., 48, 1727–1735,
777 doi:10.1021/Es404110f, 2014.
778 Chuang, P. Y., Duvall, R. M., Shafer, M. M., and Schauer, J. J.: The origin of water soluble particulate iron in
779 the Asian atmospheric outflow, Geophys. Res. Lett., 32, L07813, doi:10.1029/2004gl021946, 2005.
780 Conway, T. M. and John, S. G.: Quantification of dissolved iron sources to the North Atlantic Ocean, Nature,
781 511, 212–215, doi:10.1038/Nature13482, 2014.
782 Duce, R. A. and Tindale, N. W.: Atmospheric transport of iron and its deposition in the ocean, Limnol.
783 Oceanogr., 36, 1715–1726, 1991.
784 Espinosa, A. J. F., Rodriguez, M. T., de la Rosa, F. J. B., and Sanchez, J. C. J.: A chemical speciation of trace
785 metals for fine urban particles, Atmos. Environ., 36, 773–780, 2002.
786 Fan, S. M., Moxim, W. J., and Levy, H.: Aeolian input of bioavailable iron to the ocean, Geophys. Res. Lett.,
787 33, L07602, doi:10.1029/2005gl024852, 2006.
788 Font, O., Cordoba, P., Leiva, C., Romeo, L. M., Bolea, I., Guedea, I., Moreno, N., Querol, X., Fernandez, C.,
789 and Diez, L. I.: Fate and abatement of mercury and other trace elements in a coal fluidised bed oxy
790 combustion pilot plant, Fuel, 95, 272–281, doi:10.1016/j.fuel.2011.12.017, 2012.
791 Formenti, P., Caquineau, S., Desboeufs, K., Klaver, A., Chevaillier, S., Journet, E., and Rajot, J. L.: Mapping
792 the physico-chemical properties of mineral dust in western Africa: mineralogical composition, Atmos. Chem.
793 Phys., 14, 10663–10686, doi:10.5194/acp-14-10663-2014, 2014.
794 Fu, H. B., Lin, J., Shang, G. F., Dong, W. B., Grassian, V. H., Carmichael, G. R., Li, Y., and Chen, J. M.:
795 Solubility of iron from combustion source particles in acidic media linked to iron speciation, Environ. Sci.
796 Technol., 46, 11119–11127, doi:10.1021/Es302558m, 2012.
797 Fung, I. Y., Meyn, S. K., Tegen, I., Doney, S. C., John, J. G., and Bishop, J. K. B.: Iron supply and
798 demand in the upper ocean, Global Biogeochem. Cy., 14, 281–295, doi:10.1029/1999gb900059, 2000.
799 Gao, Y., Kaufman, Y. J., Tanre, D., Kolber, D., and Falkowski, P. G.: Seasonal distributions of aeolian iron
800 fluxes to the global ocean, Geophys. Res. Lett., 28, 29–32, doi:10.1029/2000gl011926, 2001.
801 Gerber, H.E.: Atmospheric Aerosols and Nucleation, in Lecture Notes Physics, pp. 237-238, New York,
802 1988.
803 Granier, C., Bessagnet, B., Bond, T., D'Angiola, A., van der Gon, H. D., Frost, G. J., Heil, A., Kaiser, J. W.,
804 Kinne, S., Klimont, Z., Kloster, S., Lamarque, J. F., Liousse, C., Masui, T., Meleux, F., Mieville, A., Ohara,
805 T., Raut, J. C., Riahi, K., Schultz, M. G., Smith, S. J., Thompson, A., van Aardenne, J., van der Werf, G. R.,
806 and van Vuuren, D. P.: Evolution of anthropogenic and biomass burning emissions of air pollutants at global

807 and regional scales during the 1980–2010 period, Climatic Change, 109, 163–190,
808 doi:10.1007/s10584-011-0154-1, 2011.
809 Gregg, W. W., Ginoux, P., Schopf, P. S., and Casey, N. W.: Phytoplankton and iron: validation of a global
810 three-dimensional ocean biogeochemical model, Deep-Sea Res. Pt. II, 50, 3143–3169,
811 doi:10.1016/j.dsr2.2003.07.013, 2003.
812 Grubler, A., Nakicenovic, N., and Victor, D. G.: Dynamics of energy technologies and global change, Energ.
813 Policy, 27, 247–280, doi:10.1016/S0301-4215(98)00067-6, 1999.
814 Guelle, W., Balkanski, Y. J., Schulz, M., Marticorena, B., Bergametti, G., Moulin, C., Arimoto, R., and Perry,
815 K. D.: Modeling the atmospheric distribution of mineral aerosol: comparison with ground measurements and
816 satellite observations for yearly and synoptic timescales over the North Atlantic, J. Geophys. Res.-Atmos.,
817 105, 1997–2012, doi:10.1029/1999jd901084, 2000.
818 Guieu, C., Bonnet, S., Wagener, T., and Loye-Pilot, M. D.: Biomass burning as a source of dissolved iron to
819 the open ocean?, Geophys. Res. Lett., 32, L19608, doi:10.1029/2005gl022962, 2005.
820 Hand, J. L., Mahowald, N. M., Chen, Y., Siefert, R. L., Luo, C., Subramaniam, A., and Fung, I.: Estimates of
821 atmospheric-processed soluble iron from observations and a global mineral aerosol model: biogeochemical
822 implications, J. Geophys. Res.-Atmos., 109, D17205, doi:10.1029/2004jd004574, 2004.
823 Hauglustaine, D. A., Hourdin, F., Jourdain, L., Filiberti, M. A., Walters, S., Lamarque, J. F., and Holland, E.
824 A.: Interactive chemistry in the Laboratoire de Meteorologie Dynamique general circulation model:
825 description and background tropospheric chemistry evaluation, J. Geophys. Res.-Atmos., 109, D04314,
826 doi:10.1029/2003jd003957, 2004.
827 Hildemann, L. M., Cass, G. R., and Markowski, G. R.: A dilution stack sampler for collection of organic
828 aerosol emissions–design, characterization and field-tests, Aerosol Sci. Tech., 10, 193–204,
829 doi:10.1080/02786828908959234, 1989.
830 Holscher, D., Moller, R. F., Denich, M., and Folster, H.: Nutrient input-output budget of shifting agriculture
831 in Eastern Amazonia, Nutr. Cycl. Agroecosys., 47, 49–57, 1997.
832 Hourdin, F. and Issartel, J. P.: Sub-surface nuclear tests monitoring through the CTBT xenon network,
833 Geophys. Res. Lett., 27, 2245–2248, doi:10.1029/1999gl010909, 2000.
834 Hourdin, F., Musat, I., Bony, S., Braconnot, P., Codron, F., Dufresne, J. L., Fairhead, L., Filiberti, M. A.,
835 Friedlingstein, P., Grandpeix, J. Y., Krinner, G., Levan, P., Li, Z. X., and Lott, F.: The LMDZ4 general
836 circulation model: climate performance and sensitivity to parametrized physics with emphasis on tropical
837 convection, Clim. Dynam., 27, 787–813, doi:10.1007/s00382-006-0158-0, 2006.
838 Huang, S. L., Rahn, K. A., Arimoto, R., Graustein, W. C., and Turekian, K. K.: Semi-annual cycles of
839 pollution at Bermuda, J. Geophys. Res.-Atmos., 104, 30309–30317, doi:10.1029/1999jd900801, 1999. 10
840 Huneeus, N., Schulz, M., Balkanski, Y., Griesfeller, J., Prospero, J., Kinne, S., Bauer, S., Boucher, O., Chin,
841 M., Dentener, F., Diehl, T., Easter, R., Fillmore, D., Ghan, S., Ginoux, P., Grini, A., Horowitz, L., Koch, D.,
842 Krol, M. C., Landing, W., Liu, X., Mahowald, N., Miller, R., Morcrette, J.-J., Myhre, G., Penner, J., Perlwitz,
843 J., Stier, P., Takemura, T., and Zender, C. S.: Global dust model intercomparison in AeroCom phase I, Atmos.
844 Chem. Phys., 11, 7781–7816, doi:10.5194/acp-11-7781-2011, 2011.
845 Ingerslev, M., Skov, S., Sevel, L., and Pedersen, L. B.: Element budgets of forest biomass combustion and
846 ash fertilisation – a Danish case-study, Biomass Bioenerg., 35, 2697–2704,

doi:10.1016/j.biombioe.2011.03.018, 2011.
International Energy Agency: Energy Statistics of Non-OECD Countries 1970–2006, Paris, 2008.
Ito, A.: Global modeling study of potentially bioavailable iron input from shipboard aerosol sources to the ocean, Global Biogeochem. Cy., 27, 1–10, doi:10.1029/2012gb004378, 2013.
Ito, A.: Atmospheric processing of combustion aerosols as a source of bioavailable iron, Environ. Sci. Technol. Lett., 2, 70–75, doi:10.1021/acs.estlett.5b00007, 2015.
Ito, A. and Feng, Y.: Role of dust alkalinity in acid mobilization of iron, Atmos. Chem. Phys., 10, 9237–9250, doi:10.5194/acp-10-9237-2010, 2010.
Ito, A. and Xu, L.: Response of acid mobilization of iron-containing mineral dust to improvement of air quality projected in the future, Atmos. Chem. Phys., 14, 3441–3459, doi:10.5194/acp-14-3441-2014, 2014.
Johnson, K. S., Gordon, R. M., and Coale, K. H.: What controls dissolved iron concentrations in the world ocean?, Mar. Chem., 57, 137–161, doi:10.1016/S0304-4203(97)00043-1, 1997.
Johnson, M., Edwards, R., Frenk, C. A., and Masera, O.: In-field greenhouse gas emissions from cookstoves in rural Mexican households, Atmos. Environ., 42, 1206–1222, doi:10.1016/j.atmosenv.2007.10.034, 2008.
Journet, E., Desboeufs, K. V., Caquineau, S., and Colin, J. L.: Mineralogy as a critical factor of dust iron solubility, Geophys. Res. Lett., 35, L07805, doi:10.1029/2007gl031589, 2008.
Journet, E., Balkanski, Y., and Harrison, S. P.: A new data set of soil mineralogy for dust-cycle modeling, Atmos. Chem. Phys., 14, 3801–3816, doi:10.5194/acp-14-3801-2014, 2014.
Kim, Y., Kim, N. Y., Park, S. Y., Lee, D. K., and Lee, J. H.: Classification and individualization of used engine oils using elemental composition and discriminant analysis, Forensic Sci. Int., 230, 58–67, doi:10.1016/j.forsciint.2013.01.013, 2013.
Kittelson, D. B.: Engines and nanoparticles: a review, J. Aerosol Sci., 29, 575–588, doi:10.1016/S0021-8502(97)10037-4, 1998.
Krinner, G., Viovy, N., de Noblet-Ducoudre, N., Ogee, J., Polcher, J., Friedlingstein, P., Ciais, P., Sitch, S., and Prentice, I. C.: A dynamic global vegetation model for studies of the coupled atmosphere-biosphere system, Global Biogeochem. Cy., 19, GB1015, doi:10.1029/2003gb002199, 2005.
Laclau, J. P., Sama-Poumba, W., Nzila, J. D., Bouillet, J. P., and Ranger, J.: Biomass and nutrient dynamics in a littoral savanna subjected to annual fires in Congo, Acta Oecol., 23, 41–50, doi:10.1016/S1146-609x(02)01132-3, 2002.
Lamarque, J.-F., Bond, T. C., Eyring, V., Granier, C., Heil, A., Klimont, Z., Lee, D., Liousse, C., Mieville, A., Owen, B., Schultz, M. G., Shindell, D., Smith, S. J., Stehfest, E., Van Aardenne, J., Cooper, O. R., Kainuma, M., Mahowald, N., McConnell, J. R., Naik, V., Riahi, K., and van Vuuren, D. P.: Historical (1850–2000) gridded anthropogenic and biomass burning emissions of reactive gases and aerosols: methodology and application, Atmos. Chem. Phys., 10, 7017–7039, doi:10.5194/acp-10-7017-2010, 2010.
Latva-Somppi, J., Kauppinen, E. I., Valmari, T., Ahonen, P., Gurav, A. S., Kodas, T. T., and Johanson, B.: The ash formation during co-combustion of wood and sludge in industrial fluidized bed boilers, Fuel Process. Technol., 54, 79–94, doi:10.1016/S0378-3820(97)000611, 1998.
Lee, S., Baumann, K., Schauer, J. J., Sheesley, R. J., Naeher, L. P., Meinardi, S., Blake, D. R., Edgerton, E. S., Russell, A. G., and Clements, M.: Gaseous and particulate emissions from prescribed burning in Georgia, Environ. Sci. Technol., 39, 9049–9056, doi:10.1021/Es051583l, 2005.

887 Li, X. G., Wang, S. X., Duan, L., Hao, J., Li, C., Chen, Y. S., and Yang, L.: Particulate and trace gas
888 emissions from open burning of wheat straw and corn stover in China, Environ. Sci. Technol., 41,
889 6052–6058, doi:10.1021/Es0705137, 2007.
890 Lin, Y. C., Chen, J. P., Ho, T. Y., and Tsai, I. C.: Atmospheric iron deposition in the northwestern Pacific
891 Ocean and its adjacent marginal seas: the importance of coal burning, Global Biogeochem. Cy., 29, 1–22,
892 doi:10.1002/2013GB004795, 2015.
893 Linak, W. P. and Miller, C. A.: Comparison of particle size distributions and elemental partitioning from the
894 combustion of pulverized coal and residual fuel oil, J. Air Waste Manage., 50, 1532–1544, 2000.
895 Luo, C., Mahowald, N. M., and del Corral, J.: Sensitivity study of meteorological parameters on mineral
896 aerosol mobilization, transport, and distribution, J. Geophys. Res.-Atmos., 108, 4447,
897 doi:10.1029/2003jd003483, 2003.
898 Luo, C., Mahowald, N. M., Meskhidze, N., Chen, Y., Siefert, R. L., Baker, A. R., and Johansen, A. M.:
899 Estimation of iron solubility from observations and a global aerosol model, J. Geophys. Res.-Atmos., 110,
900 4447, doi:10.1029/2005jd006059, 2005.
901 Luo, C., Mahowald, N., Bond, T., Chuang, P. Y., Artaxo, P., Siefert, R., Chen, Y., and Schauer, J.:
902 Combustion iron distribution and deposition, Global Biogeochem. Cy., 22, D23307,
903 doi:10.1029/2007gb002964, 2008.
904 Mackensen, J., Holscher, D., Klinge, R., and Folster, H.: Nutrient transfer to the atmosphere by burning of
905 debris in eastern Amazonia, Forest Ecol. Manag., 86, 121–128, doi:10.1016/S0378-1127(96)03790-5, 1996.
906 Mahowald, N. M., Baker, A. R., Bergametti, G., Brooks, N., Duce, R. A., Jickells, T. D., Kubilay, N.,
907 Prospero, J. M., and Tegen, I.: Atmospheric global dust cycle and iron inputs to the ocean, Global
908 Biogeochem. Cy., 19, GB1012, doi:10.1029/2004gb002402, 2005.
909 Mahowald, N. M., Engelstaedter, S., Luo, C., Sealy, A., Artaxo, P., Benitez-Nelson, C., Bonnet, S., Chen, Y.,
910 Chuang, P. Y., Cohen, D. D., Dulac, F., Herut, B., Johansen, A. M., Kubilay, N., Losno, R., Maenhaut, W.,
911 Paytan, A., Prospero, J. A., Shank, L. M., and Siefert, R. L.: Atmospheric iron deposition: global distribution,
912 variability, and human perturbations, Annu. Rev. Mar. Sci., 1, 245–278,
913 doi:10.1146/annurev.marine.010908.163727, 2009.
914 Mahowald, N., Lindsay, K., Rothenberg, D., Doney, S. C., Moore, J. K., Thornton, P., Randerson, J. T., and
915 Jones, C. D.: Desert dust and anthropogenic aerosol interactions in the Community Climate System Model
916 coupled-carbon-climate model, Biogeosciences, 8, 387–414, doi:10.5194/bg-8-387-2011, 2011.
917 Mamane, Y., Miller, J. L., and Dzubay, T. G.: Characterization of individual fly-ash particles emitted from
918 coal-fired and oil-fired power-plants, Atmos. Environ., 20, 2125–2135, doi:10.1016/0004-6981(86)90306-9,
919 1986.
920 Martin, J. H.: Glacial-interglacial CO_2 change: the iron hypothesis, Paleoceanography, 5, 1–13,
921 doi:10.1029/Pa005i001p00001, 1990.
922 Martin, J. H., Gordon, R. M., and Fitzwater, S. E.: The case for iron, Limnol. Oceanogr., 36, 1793–1802,
923 1991.
924 Meij, R.: Trace-element behavior in coal-fired power-plants, Fuel Process. Technol., 39, 199–217,
925 doi:10.1016/0378-3820(94)90180-5, 1994.
926 Mestdagh, M. M., Vielvoye, L., and Herbillon, A. J.: Iron in Kaolinite: The relationship between kaolinite

crystallinity and iron content, Clay Minerals, 15, 1–13, 1980.
Ministry of Environmental Protection of the People's Republic of China: China Environment Yearbook 2008, China Environment Yearbook Inc., Beijing, 2008.
Moore, C. M., Mills, M. M., Arrigo, K. R., Berman-Frank, I., Bopp, L., Boyd, P. W., Galbraith, E. D., Geider, R. J., Guieu, C., Jaccard, S. L., Jickells, T. D., La Roche, J., Lenton, T. M., Mahowald, N. M., Maranon, E., Marinov, I., Moore, J. K., Nakatsuka, T., Oschlies, A., Saito, M. A., Thingstad, T. F., Tsuda, A., and Ulloa, O.: Processes and patterns of oceanic nutrient limitation, Nat. Geosci., 6, 701–710, doi:10.1038/Ngeo1765, 2013.
Moore, J. K., Doney, S. C., and Lindsay, K.: Upper ocean ecosystem dynamics and iron cycling in a global three-dimensional model, Global Biogeochem. Cy., 18, GB4025, doi:10.1029/2004gb002220, 2004.
Narodoslawsky, M. and Obernberger, I.: From waste to raw material – the route from biomass to wood ash for cadmium and other heavy metals, J. Hazard. Mater., 50, 157–168, doi:10.1016/0304-3894(96)01785-2, 1996.
Murad, E. and Wagner, U.: The Mossbauer spectrum of illite, Clay Minerals, 29, 1–10, 1994.
Nickovic, S., Vukovic, A., Vujadinovic, M., Djurdjevic, V., and Pejanovic, G.: Technical Note: High-resolution mineralogical database of dust-productive soils for atmospheric dust modeling, Atmos. Chem. Phys., 12, 845–855, doi:10.5194/acp-12-845-2012, 2012.
Nickovic, S., Vukovic, A., and Vujadinovic, M.: Atmospheric processing of iron carried by mineral dust, Atmos. Chem. Phys., 13, 9169–9181, doi:10.5194/acp-13-9169-2013, 2013.
Olmez, I., Sheffield, A. E., Gordon, G. E., Houck, J. E., Pritchett, L. C., Cooper, J. A., Dzubay, T. G., and Bennett, R. L.: Compositions of particles from selected sources in Philadelphia for receptor modeling applications, JAPCA J. Air Waste Ma., 38, 1392–1402, 1988.
Pivello, V. R. and Coutinho, L. M.: Transfer of macro-nutrients to the atmosphere during experimental burnings in an open cerrado (Brazilian Savanna), J. Trop. Ecol., 8, 487–497, doi:10.1017/S0266467400006829, 1992.
Querol, X., Fernandez-Turiel, J. L., and Lopez Soler, A.: Trace-elements in coal and their behavior during combustion in a large power-station, Fuel, 74, 331–343, doi:10.1016/0016-2361(95)93464-O, 1995.
Raison, R. J., Khanna, P. K., and Woods, P. V.: Mechanisms of element transfer to the atmosphere during vegetation fires, Can. J. Forest Res., 15, 132–140, doi:10.1139/X85-022, 1985.
Reddy, M. S., Basha, S. B., Joshi, H. V., and Jha, B.: Evaluation of the emission characteristics of trace metals from coal and fuel oil fired power plants and their fate during combustion, J. Hazard. Mater., 123, 242–249, doi:10.1016/j.jhazmat.2005.04.008, 2005.
Ridgwell, A. J. and Watson, A. J.: Feedback between aeolian dust, climate, and atmospheric CO_2 in glacial time, Paleoceanography, 17, GB4028, doi:10.1029/2001pa000729, 2002.
Sager, M.: Trace and nutrient elements in manure, dung and compost samples in Austria, Soil Biol. Biochem., 39, 1383–1390, doi:10.1016/j.soilbio.2006.12.015, 2007.
Schroth, A. W., Crusius, J., Sholkovitz, E. R., and Bostick, B. C.: Iron solubility driven by speciation in dust sources to the ocean, Nat. Geosci., 2, 337–340, doi:10.1038/Ngeo501, 2009.
Schulz, M.: Constraining Model Estimates of the Aerosol Radiative Forcing, Thèse d'Habilitation à Diriger des Recherches, Université Pierre et Marie Curie, Paris VI, 2007.
Schulz, M., Balkanski, Y. J., Guelle, W., and Dulac, F.: Role of aerosol size distribution and source location

967 in a three-dimensional simulation of a Saharan dust episode tested against satellite-derived optical thickness,
968 J. Geophys. Res.-Atmos., 103, 10579–10592, doi:10.1029/97jd02779, 1998.
969 Schultz, M. G., Heil, A., Hoelzemann, J. J., Spessa, A., Thonicke, K., Goldammer, J. G., Held, A. C., Pereira,
970 J. M. C., and van het Bolscher, M.: Global wildland fire emissions from 1960 to 2000, Global Biogeochem.
971 Cy., 22, 1059, doi:10.1029/2007gb003031, 2008.
972 Schulz, M., Prospero, J. M., Baker, A. R., Dentener, F., Ickes, L., Liss, P. S., Mahowald, N. M., Nickovic, S.,
973 Garcia-Pando, C. P., Rodriguez, S., Sarin, M., Tegen, I., and Duce, R. A.: Atmospheric transport and
974 deposition of mineral dust to the ocean: implications for research needs, Environ. Sci. Technol., 46,
975 10390–10404, doi:10.1021/Es300073u, 2012.
976 Sedwick, P. N., Sholkovitz, E. R., and Church, T. M.: Impact of anthropogenic combustion emissions on the
977 fractional solubility of aerosol iron: evidence from the Sargasso Sea, Geochem. Geophy. Geosy., 8, Q10Q06,
978 doi:10.1029/2007gc001586, 2007.
979 Shen, G. F., Yang, Y. F., Wang, W., Tao, S., Zhu, C., Min, Y. J., Xue, M. A., Ding, J. N., Wang, B., Wang, R.,
980 Shen, H. Z., Li, W., Wang, X. L., and Russell, A. G.: Emission factors of particulate matter and elemental
981 carbon for crop residues and coals burned in typical household stoves in China, Environ. Sci. Technol., 44,
982 7157–7162, doi:10.1021/Es101313y, 2010.
983 Shen, G. F., Wei, S. Y., Wei, W., Zhang, Y. Y., Min, Y. J., Wang, B., Wang, R., Li, W., Shen, H. Z., Huang, Y.,
984 Yang, Y. F., Wang, W., Wang, X. L., Wang, X. J., and Tao, S.: Emission factors, size distributions, and
985 emission inventories of carbonaceous particulate matter from residential wood combustion in rural China,
986 Environ. Sci. Technol., 46, 4207–4214, doi:10.1021/Es203957u, 2012.
987 Sholkovitz, E. R., Sedwick, P. N., and Church, T. M.: Influence of anthropogenic combustion emissions on
988 the deposition of soluble aerosol iron to the ocean: empirical estimates for island sites in the North Atlantic,
989 Geochim. Cosmochim. Ac., 73, 3981–4003, doi:10.1016/j.gca.2009.04.029, 2009.
990 Sholkovitz, E. R., Sedwick, P. N., Church, T. M., Baker, A. R., and Powell, C. F.: Fractional solubility of
991 aerosol iron: synthesis of a global-scale data set, Geochim. Cosmochim. Ac., 89, 173–189,
992 doi:10.1016/j.gca.2012.04.022, 2012.
993 Slinn, S. A. and Slinn, W. G. N.: Predictions for particle deposition on natural waters, Atmos. Environ., 14,
994 1013–1016, doi:10.1016/0004-6981(80)90032-3, 1980.
995 Smith, R. D., Campbell, J. A., and Nielson, K. K.: Characterization and formation of submicron particles in
996 coal-fired plants, Atmos. Environ., 13, 607–617, doi:10.1016/00046981(79)90189-6, 1979.
997 Sun, Y. L., Zhuang, G. S., Ying, W., Han, L. H., Guo, J. H., Mo, D., Zhang, W. J., Wang, Z. F., and Hao, Z. P.:
998 The air-borne particulate pollution in Beijing – concentration, composition, distribution and sources, Atmos.
999 Environ., 38, 5991–6004, doi:10.1016/j.atmosenv.2004.07.009, 2004.
1000 Tagliabue, A., Bopp, L., and Aumont, O.: Evaluating the importance of atmospheric and sedimentary iron
1001 sources to Southern Ocean biogeochemistry, Geophys. Res. Lett., 36, Q10Q06, doi:10.1029/2009gl038914,
1002 2009.
1003 Tang, Q., Liu, G. J., Zhou, C. C., and Sun, R. Y.: Distribution of trace elements in feed coal and combustion
1004 residues from two coal-fired power plants at Huainan, Anhui, China, Fuel, 107, 315–322,
1005 doi:10.1016/j.fuel.2013.01.009, 2013.
1006 Taylor, S. R. and McLennan, S. M.: The Continental Crust: Its Composition and Evolution, Blackwell,

Malden, MA, 312 pp., 1985.
Tegen, I. and Fung, I.: Modeling of mineral dust in the atmosphere– sources, transport, and optical-thickness, J. Geophys. Res.-Atmos., 99, 22897–22914, doi:10.1029/94jd01928, 1994.
Tewalt, S. J., Belkin, H. E., SanFilipo, J. R., Merrill, M. D., Palmer, C. A., Warwick, P. D., Karlsen, A. W., Finkelman, R. B., and Park, A. J.: Chemical analyses in the World coal quality inventory, version 1: U. S. Geological Survey Open-File Report 2010-1196, available at: http://pubs.usgs.gov/of/2010/1196/ (last access: 10 March 2015), 2010.
Valmari, T., Lind, T. M., Kauppinen, E. I., Sfiris, G., Nilsson, K., and Maenhaut, W.: Field study on ash behavior during circulating fluidized-bed combustion of biomass. 1. Ash formation, Energ. Fuel., 13, 379–389, doi:10.1021/Ef980085d, 1999.
van der Werf, G. R., Randerson, J. T., Giglio, L., Collatz, G. J., Mu, M., Kasibhatla, P. S., Morton, D. C., DeFries, R. S., Jin, Y., and van Leeuwen, T. T.: Global fire emissions and the contribution of deforestation, savanna, forest, agricultural, and peat fires (1997–2009), Atmos. Chem. Phys., 10, 11707–11735, doi:10.5194/acp-10-11707-2010, 2010.
Vassilev, S. V., Baxter, D., Andersen, L. K., and Vassileva, C. G.: An overview of the chemical composition of biomass, Fuel, 89, 913–933, doi:10.1016/j.fuel.2009.10.022, 2010.
Vestreng, V., Myhre, G., Fagerli, H., Reis, S., and Tarrasón, L.: Twenty-five years of continuous sulphur dioxide emission reduction in Europe, Atmos. Chem. Phys., 7, 3663–3681, doi:10.5194/acp-7-3663-2007, 2007.
Wang, R., Tao, S., Ciais, P., Shen, H. Z., Huang, Y., Chen, H., Shen, G. F., Wang, B., Li, W., Zhang, Y. Y., Lu, Y., Zhu, D., Chen, Y. C., Liu, X. P., Wang, W. T., Wang, X. L., Liu, W. X., Li, B. G., and Piao, S. L.: High-resolution mapping of combustion processes and implications for CO_2 emissions, Atmos. Chem. Phys., 13, 5189–5203, doi:10.5194/acp-13-5189-2013, 2013.
Wang, R., Tao, S., Shen, H. Z., Huang, Y., Chen, H., Balkanski, Y., Boucher, O., Ciais, P., Shen, G. F., Li, W., Zhang, Y. Y., Chen, Y. C., Lin, N., Su, S., Li, B. G., Liu, J. F., and Liu, W. X.: Trend in global black carbon emissions from 1960 to 2007, Environ. Sci. Technol., 48, 6780–6787, doi:10.1021/Es5021422, 2014a.
Wang, R., Tao, S., Balkanski, Y., Ciais, P., Boucher, O., Liu, J. F., Piao, S. L., Shen, H. Z., Vuolo, M. R., Valari, M., Chen, H., Chen, Y. C., Cozic, A., Huang, Y., Li, B. G., Li, W., Shen, G. F., Wang, B., and Zhang, Y. Y.: Exposure to ambient black carbon derived from a unique inventory and high-resolution model, P. Natl. Acad. Sci. USA, 111, 2459–2463, doi:10.1073/pnas.1318763111, 2014b.
Wang, R., Balkanski, Y., Boucher, O., Ciais, P., Penuelas, J., and Tao, S.: Significant contribution of combustion-related emissions to the atmospheric phosphorus budget, Nat. Geosci., 1, 48–54, 2015.
Wang, Y. F., Huang, K. L., Li, C. T., Mi, H. H., Luo, J. H., and Tsai, P. J.: Emissions of fuel metals content from a diesel vehicle engine, Atmos. Environ., 37, 4637–4643, doi:10.1016/j.atmosenv.2003.07.007, 2003.
Yen, C.: High volume fly ash concrete manufacturing technique and application study, Technical Report for the Taiwan Power Company, 275 pp., Taipei, Taiwan, 2011.
Yi, H. H., Hao, J. M., Duan, L., Tang, X. L., Ning, P., and Li, X. H.: Fine particle and trace element emissions from an anthracite coal-fired power plant equipped with a bag-house in China, Fuel, 87, 2050–2057, doi:10.1016/j.fuel.2007.10.009, 2008.
Zhang, H. F., Ye, X. N., Cheng, T. T., Chen, J. M., Yang, X., Wang, L., and Zhang, R. Y.: A laboratory study

of agricultural crop residue combustion in China: emission factors and emission inventory, Atmos. Environ., 42, 8432–8441, doi:10.1016/j.atmosenv.2008.08.015, 2008.

Zhao, Y., Wang, S., Duan, L., Lei, Y., Cao, P., and Hao, J.: Primary air pollutant emissions of coal-fired power plants in China: Current status and future prediction. Atmos. Environ., 42(36), 8442-8452, 2008.

Tables

Table 1. Parameters used in the estimation of Fe emissions from combustion sources.

Parameter	Description	Values or data sources
a	Fuel consumption	The fuel data was taken from a global 0.1°×0.1° fuel data set which is used to construct a global CO_2 emission inventory (Wang et al., 2013; available at http://inventory.pku.edu.cn/home.html).
b	Completeness of combustion	n coal (98%); n petroleum (98%); n wood in stoves (88%); n wood in fireplaces (79%); n crop residues (92%); n biomass burning (considered in van der Werf, 2010).
c	Fe content of the fuel	n coal: based on Fe contents in coal produced by country (**Table S2**) and an international coal-trading matrix (Chen et al., 2014); n wood (a geometric mean of 0.036% and range in **Fig. S1**); n crop residues (a geometric mean of 0.060% and range in **Fig. S1**); n grass (a geometric mean of 0.027% and range in **Fig. S1**); n dung cakes (0.13±0.09 %); n biodiesel (0.00024±0.00023 %); n heavy fuel oil (32±2 ppm); n diesel (13±7 ppm); n gasoline (3.3±2.6 ppm); n liquefied petroleum gas (4.9±3.3 ppm).
f	Fraction of Fe retained in residue ash relative to the amount of Fe in the burnt fuel	n coal used in industry and power plants (30-45%); n petroleum used in industry and power plants (43-58%); n solid biofuels used in industry and power plants (60-70%); n petroleum consumed by motor vehicles (2-12%); n anthracite coal used in the residential sector (99.2-99.8%); n bituminous coal used in the residential sector (91-97%); n crop residues used in the residential sector (79-95%); n wood used in the residential sector (89-99%); n forest fires (49-98%); n savanna fires (24-79%); n deforestation (43-50%); n woodland fires / peat fires (41-56%).
J_x	Fraction of Fe emitted in a particle size	n coal fly ash (0.1-0.3% in PM_1; 10-30% in PM_{1-10}; the remainder in $PM_{>10}$); n oil fly ash (80-95% in PM_1; the remainder in PM_{1-10}); n biomass fly ash (1-3% in PM_1; 50-60% in PM_{1-10}; the remainder in $PM_{>10}$).
A_y	Fraction of a specific control device	A_y is computed for each country and each year using a function by Grubler et al. (1999) and Bond et al. (2007): $A_y = (F_0\text{-}F_f) \exp [-(t\text{-}t_0)2/2s^2] + F_f$, where F_0 and F_f are the initial and final fractions of the technology, t_0 is transition beginning time, and s is transition rate. Parameters were determined for developing or developed countries and listed in Wang et al. (2014a).
$R_{x,y}$	Removal efficiency for each particle size by different control device (Zhao et al., 2008)	n cyclone (10% for PM_1; 70% for PM_{1-10}; 90% for $PM_{>10}$); n scrubber (50% for PM_1; 90% for PM_{1-10}; 99% for $PM_{>10}$); n electrostatic precipitator (93.62% for PM_1; 97.61% for PM_{1-10}; 99.25% for $PM_{>10}$).

Table 2. Comparison of Fe emissions from combustion and mineral sources (Tg yr^{-1}) in the present work and previous studies. The uncertainty range in our estimate is given in bracket as a 90% confidence interval from a Monte Carlo simulation (1000 runs). The Fe content of dust used to estimate Fe emissions from mineral sources (F_c) is indicated for each estimate.

Study	Year (s)	Fossil fuels	Biomass	Mineral sources
Bertine and Goldberg, 1971	1967	1.4 (all sizes)		
Luo et al., 2008	1996	0.56 (PM_{1-10})	0.86 (PM_{1-10})	55 (F_c =3.5%)
		0.10 (PM_1)	0.21 (PM_1)	
Ito, 2013	2001	0.44 (PM_{1-10})	0.92 (PM_{1-10})	74 (F_c =3.5%)
		0.07 (PM_1)	0.23 (PM_1)	
Present study	1967	3.0 (1.2-7.2) (all sizes)		
	1996	1.1 (0.54-2.4) (PM_{1-10})	0.46 (0.16-1.27) (PM_{1-10})	
		0.036 (0.022-0.060) (PM_1)	0.017 (0.006-0.046) (PM_1)	
	2001	0.83 (0.40-1.7) (PM_{1-10})	0.46 (0.16-1.26) (PM_{1-10})	
		0.035 (0.022-0.058) (PM_1)	0.017 (0.006-0.046) (PM_1)	
	2000-2011			38.5 (F_c =3.5%)
	2000-2011			41.0 (F_c using new mineralogical data)

Table 3. Statistics for the comparison of modelled and observed Fe concentrations. *N*, sample size; F_2 and F_5, fractions of stations with deviations within a factor of two or five, respectively; *NMB*, normalized mean bias. The values in brackets show the indicators when the combustion sources are not included.

	N	***F_2* (%)**	***F_5* (%)**	***NMB* (%)**
Indian Ocean	61	30 (30)	75 (75)	-68 (-68)
Atlantic Ocean	224	64 (63)	83 (79)	15 (14)
Pacific Ocean	126	52 (48)	69 (67)	-66 (-69)
South Ocean	47	47 (36)	53 (43)	-44 (-79)
East Asia	32	84 (13)	100 (31)	-1.4 (-78)
South America	4	75 (50)	100 (50)	-73 (-91)
North America	12	83 (33)	100 (67)	-39 (-66)
Mediterranean	23	61 (57)	87 (87)	24 (16)
All regions	**529**	**57 (49)**	**78 (70)**	**-14 (-32)**

Table 4. Global Fe budgets from various sources and from different particle size classes. The total deposition of Fe was calculated over land and oceans separately, and was also calculated for the dry deposition (DRY), wet deposition (WET), and sedimentation (SED), respectively.

	Source ($Tg\ yr^{-1}$)	**Burden (Gg)**	**Lifetime (days)**	**Deposition ($Tg\ yr^{-1}$)**		**Deposition ($Tg\ yr^{-1}$)**		
				Over land	**Over ocean**	**DRY**	**WET**	**SED**
Coal								
PM_1	0.018	0.262	5.28	0.013	0.005	0.008	0.010	0.0002
PM_{1-10}	1.025	6.437	2.30	0.807	0.215	0.310	0.331	0.381
$PM_{>10}$	3.167	0.431	0.05	2.905	0.235	0.142	0.026	2.971
Total	**4.210**	**7.131**	**0.26**	**3.724**	**0.455**	**0.460**	**0.367**	**3.352**
Petroleum								
PM_1	0.020	0.289	5.20	0.010	0.010	0.007	0.013	0.0002
PM_{1-10}	0.002	0.014	2.22	0.001	0.001	0.001	0.001	0.001
Total	**0.022**	**0.303**	**4.79**	**0.011**	**0.011**	**0.008**	**0.014**	**0.001**
Biomass								
PM_1	0.018	0.466	9.40	0.012	0.006	0.006	0.010	0.0003
PM_{1-10}	0.482	5.303	4.12	0.367	0.103	0.130	0.184	0.154
$PM_{>10}$	0.375	0.083	0.08	0.353	0.013	0.017	0.004	0.344
Total	**0.875**	**5.852**	**1.27**	**0.731**	**0.122**	**0.154**	**0.199**	**0.498**
Dust	**41.0**	**442**	**3.95**	**33.0**	**7.82**	**15.3**	**15.1**	**10.4**

Figure Captions

Figure 1. Frequency distributions of Fe emissions from different fuel types (**A**) and particle sizes (**B**). The distributions are derived from 1000 Monte Carlo simulations. The standard deviation of $\log_{10}$-transformed Fe emissions is shown for each distribution. The x-axis is plotted on a log scale.

Figure 2. Source profiles of Fe from combustion for PM_1 (**A**), $PM_{1\text{-}10}$ (**B**), and $PM_{>10}$ (**C**) as an average for 1960-2007. The total Fe emission for each size class is provided under its pie chart.

Figure 3. Spatial distributions of Fe emissions from combustion sources in 2007 at a resolution of 0.1° × 0.1° for fine (PM_1) (**A**) and medium-to-coarse ($PM_{1\text{-}10}$ and $PM_{>10}$) (**B**) particles.

Figure 4. Temporal trends of Fe emissions of fine (PM_1) (**A**) and medium-to-coarse ($PM_{1\text{-}10}$ and $PM_{>10}$) (**B**) particles from combustion sources from 1960 to 2007. Fe emissions from wildfires are shown separately with energy-related activities separated by region (NA for North America and SA for South America).

Figure 5. Average Fe emission from dust sources for 2000-2011 using the new mineralogical data set (**A**) and the difference of average Fe emission from dust sources for 2000-2011 using the new mineralogical data set relative to that using a constant Fe content (3.5%) (**B**). A positive value in (**B**) indicates a larger emission density by using the new mineralogical data set.

Figure 6. Distribution of annual mean concentrations of Fe attached to aerosols in surface air. A total of 529 measured Fe concentrations compiled by Mahowald et al. (2009) and Sholkovitz et al. (2012) and collected in this study (**Table S3**) are shown as circles, and a total of 296 Fe concentrations measured by Baker et al. (2013) over the Atlantic Ocean are shown as triangles.

Figure 7. Comparisons of modelled and observed Fe concentrations by region (**A**) and measuring type (**B**). The modelled concentrations are averaged for the months in the year of measuring. The fitted curves for all stations in (**A**) and long-term measurement stations in (**B**) are shown as red dashed lines, with coefficients of determination (r^2) listed. The 1:1 (solid), 1:2 and 2:1 (dashed), and 1:5 and 5:1 (dotted) lines are shown.

Figure 8. Comparisons of modelled and measured Fe concentrations. The Fe concentrations were derived as monthly (blue triangles) or daily (orange triangles) means from the model. (**A**) Fe measured in autumn 2001 (James Clark Ross (JCR) cruise) by Baker

et al. (2006). (**B**) Fe measured in winter 2001 by Chen and Siefert (2004). (**C**) Fe measured in summer 2001 by Chen and Siefert (2004). (**D**) Fe measured in spring 2003 by Chen and Siefert (2004). (**E**) Locations of the cruise measurements (**A**-**D**).

Figure 9. Zonal distribution of modelled (cyan dots) and measured (black dots) Fe concentrations attached to aerosols in surface air over the Atlantic Ocean from 70°S to 60°N. The solid lines with circles show the modelled (blue) and measured (black) Fe concentrations as geometric means in each band with error bars for the geometric standard deviations. As sensitivity tests, Fe concentrations from mineral sources were scaled by factors of 0.32 and 2.12 (solid and dashed red lines) as 90% uncertainties in dust emissions (Huneeus et al., 2011) and Fe concentrations from combustion sources were scaled by factors of 0.44 and 2.27 (solid and dashed green lines) as 90% uncertainties in Fe emissions from combustion.

Figure 10. Seasonality of Fe concentrations attached to aerosols in surface air at Bermuda (32.2°N, 64.5°W) (**A**) and Barbados (13.2°N, 59.3°W) (**B**) on the western margin of the Atlantic Ocean. Modelled Fe concentrations are derived from all sources (Fe_total) and from mineral sources only (Fe_dust) as medians of all days for the month of 2005. Measured Fe concentrations are shown as the medians (circles) for 1988-1994 with the ranges between the 10^{th} and 90^{th} percentiles (error bars).

Figure 11. Relative contribution of combustion sources to the modelled Fe concentrations attached to aerosols in surface air.

Figure 12. Plots of modelled and measured Fe concentrations attached to aerosols in surface air with (**A**) or without (**B**) combustion sources. All stations were divided into four groups based on the contribution of combustion sources: G1, contribution ≥50% (blue triangles); G2, 30%≤ contribution <50% (red triangles); G3: 15%≤ contribution <30% (green triangles); G4, contribution <15% (grey squares). The ratios between measured and modelled concentrations as geometric means are listed with the number of stations in the brackets for each group. The fitted curves for the G1 stations are shown as blue lines with coefficients of determination (r^2).

Figure 13. Relative differences in simulated Fe concentrations attached to aerosols in surface air when using the new mineralogical data and prescribing a constant Fe content in dust (3.5%). A positive difference indicates a higher Fe concentration when using the new mineralogical data.

Figure 14. Plots of modelled and measured Fe concentrations attached to aerosols in surface air. The Fe content of dust was calculated from the new mineralogical data (**A**) or prescribed as 3.5% (**B**). All stations were divided into four groups based on the

relative differences between **A** and **B**: G1, difference ≥ 30% (blue triangles); G2, 20% ≤ difference < 30% (red triangles); G3: 10% ≤ difference < 20% (green triangles); G4, difference < 10% (grey squares). The ratios between measured and modelled concentrations as geometric means are listed with the number of stations in brackets for each group.

Figure 15. Spatial distributions of the wet mass median diameter (μm) of Fe-containing particles in surface air. **A,** Fe from all combustion and mineral sources. **B-D**, Fe from coal combustion in PM_1 (**B**), PM_{1-10}(**C**), and $PM_{>10}$ (**D**). The global mean is provided in each panel.

Figure 16. Global distribution of modelled annual mean Fe deposition rates. The observed Fe deposition rates from *in situ* measurements compiled by Mahowald et al. (2009) are shown as diamonds of the same color as the scale.

Figure 17. Relative contributions of atmospheric Fe deposition over oceans by mineral sources (**A**) and combustion of coal (**B**), oil (**C**), and biomass (**D**). The average contribution over the oceans and the measured Fe solubility are provided in the panel descriptions. Color scales differ on each plot.

Figure 18. Relative contribution of combustion-related emissions to atmospheric soluble Fe deposition over oceans. Constant Fe solubilities (0.44% for dust, 22.5% for coal fly ash, 79% for oil fly ash and 18% for biomass fly ash) were applied to calculate the deposition of soluble Fe from the deposition of total Fe.

Figure 19. Comparison of modelled and observed soluble Fe concentrations over the Atlantic (**A**) and Pacific (**B**) Oceans. Model simulations were run for 2004 and 2005 with the Fe emissions from mineral dust, but without (grey squares) or with (red triangles) the emissions from combustion. Fixed Fe solubilities were applied for Fe from mineral dust (0.44%) and combustion of coal (22.5%), oil (79%) and biomass (18%). The measured daily soluble Fe concentrations in 2004 and 2005 were compiled from the literature (Baker et al., 2007; Sedwick et al., 2007; Buck et al., 2006; Buck et al., 2010). The modelled and observed soluble Fe concentrations were compared on the same days. To evaluate the model performance, the root mean square deviations (RMSD) are computed for $\log_{10}$-transformed concentrations. The 1:1 (solid), 1:2 and 2:1 (dashed), and 1:5 and 5:1 (dotted) lines are shown. Locations of the measurement sites are shown in (**C**).

Figures

Fig. 1

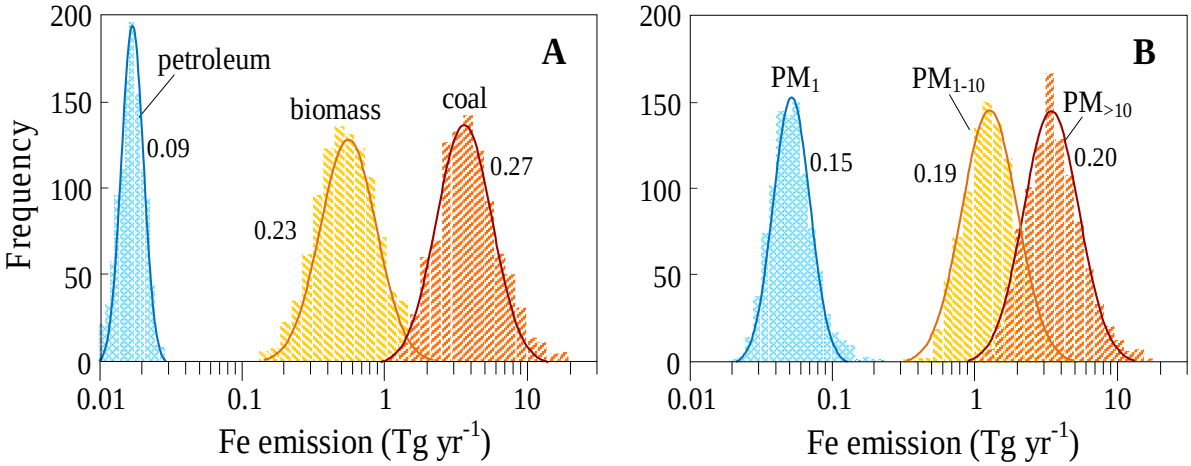

1176 Fig. 2

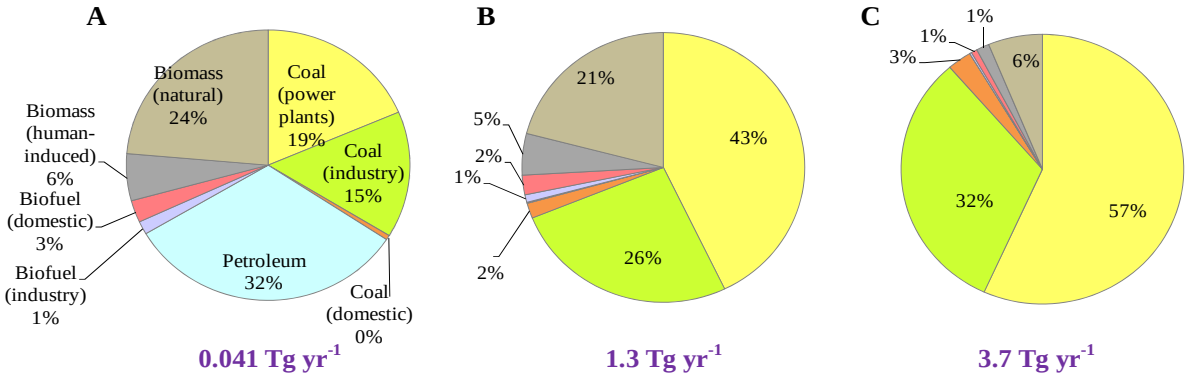

1177

1178

1179 Fig. 3

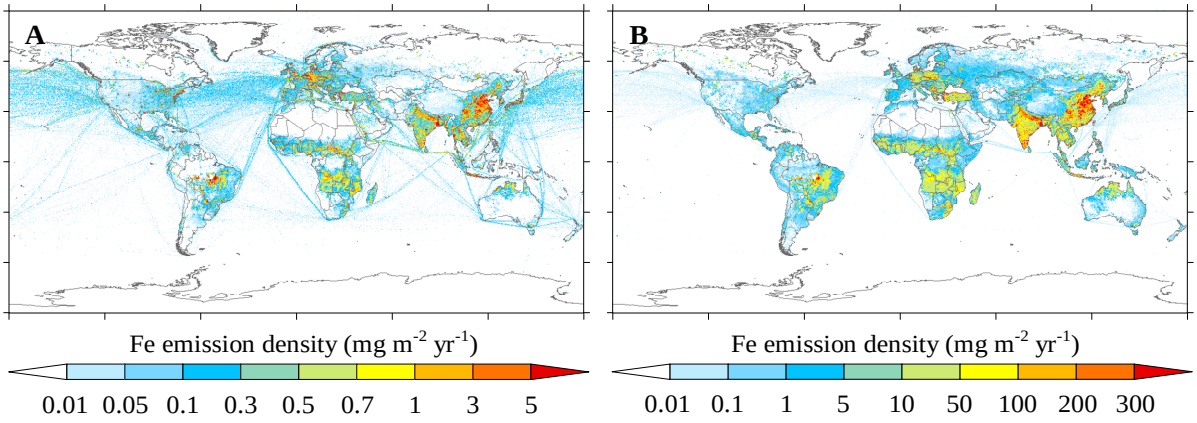

1180

1181

1182 Fig. 4

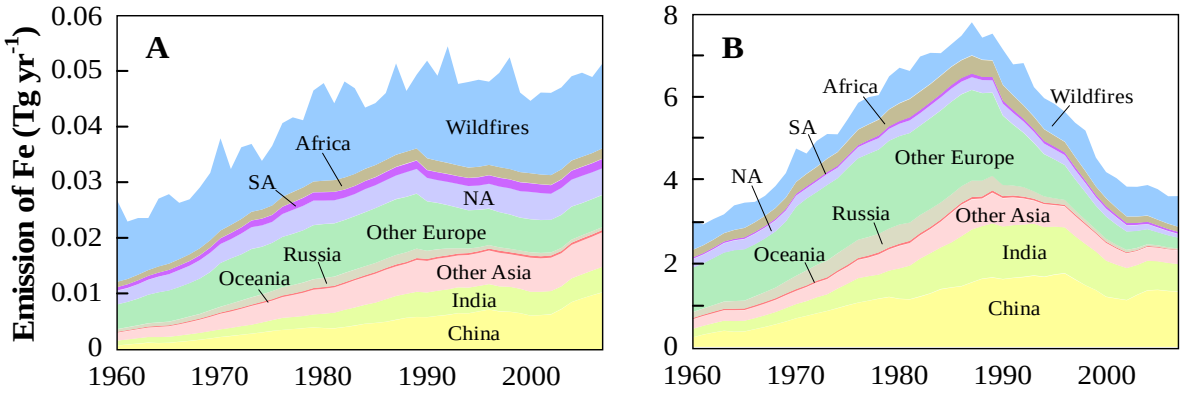

1183

1184

1185 Fig. 5

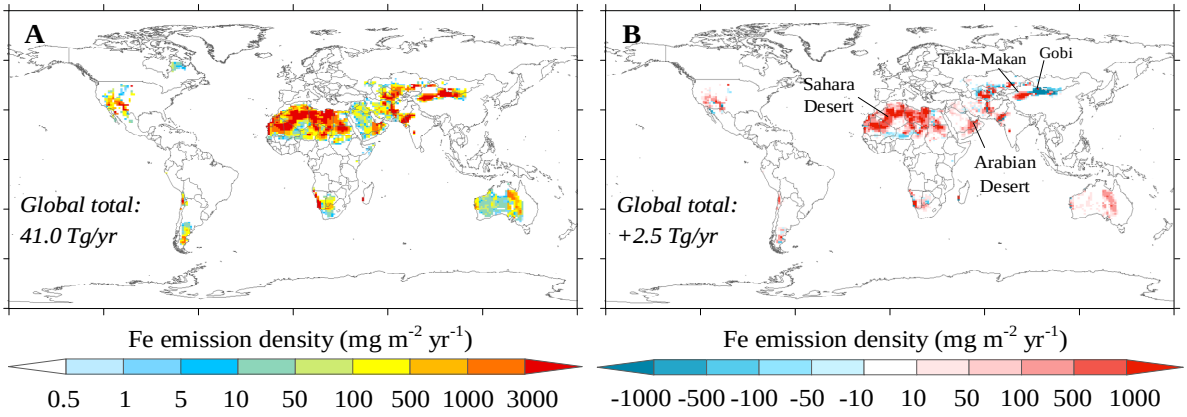

1186

1187

1188 Fig. 6

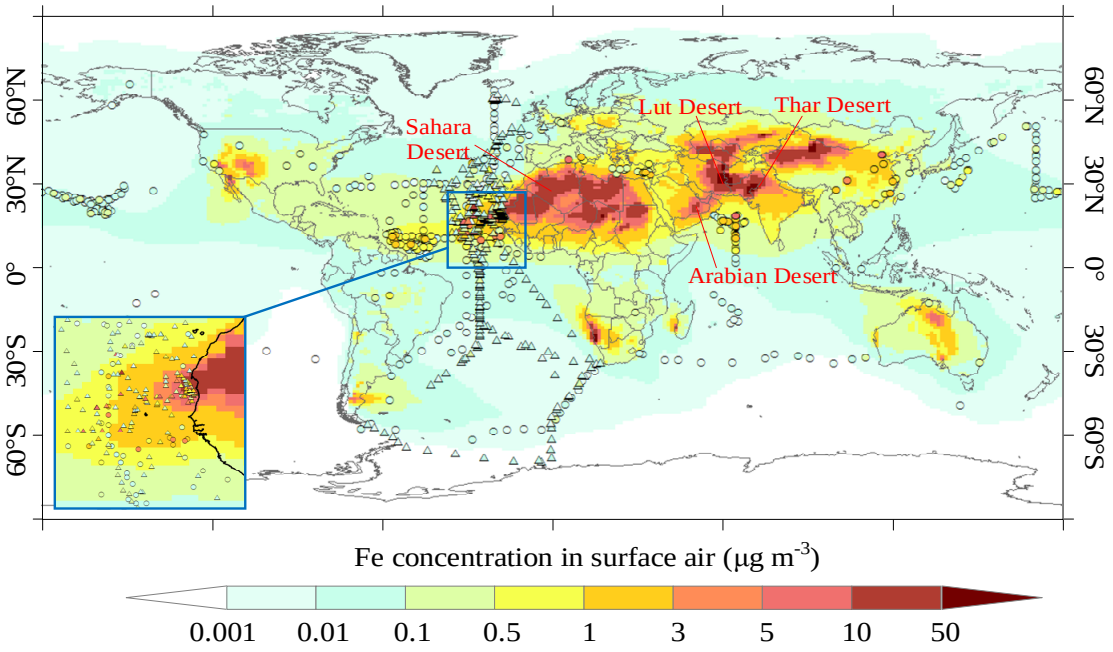

1189

1190

1191 Fig. 7

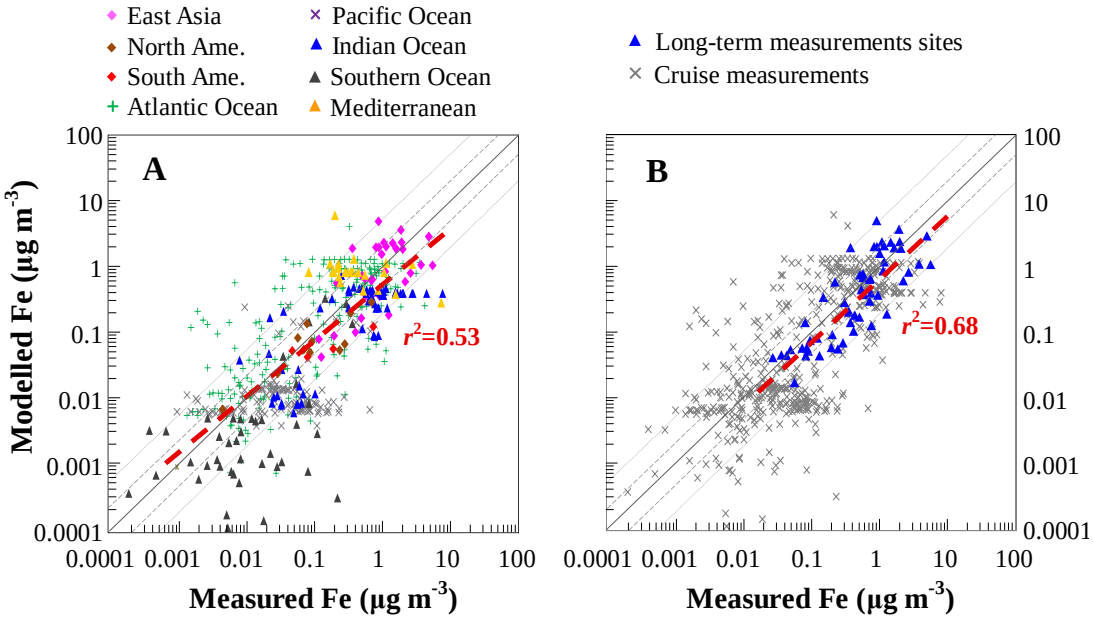

1192

1193

1194 Fig. 8

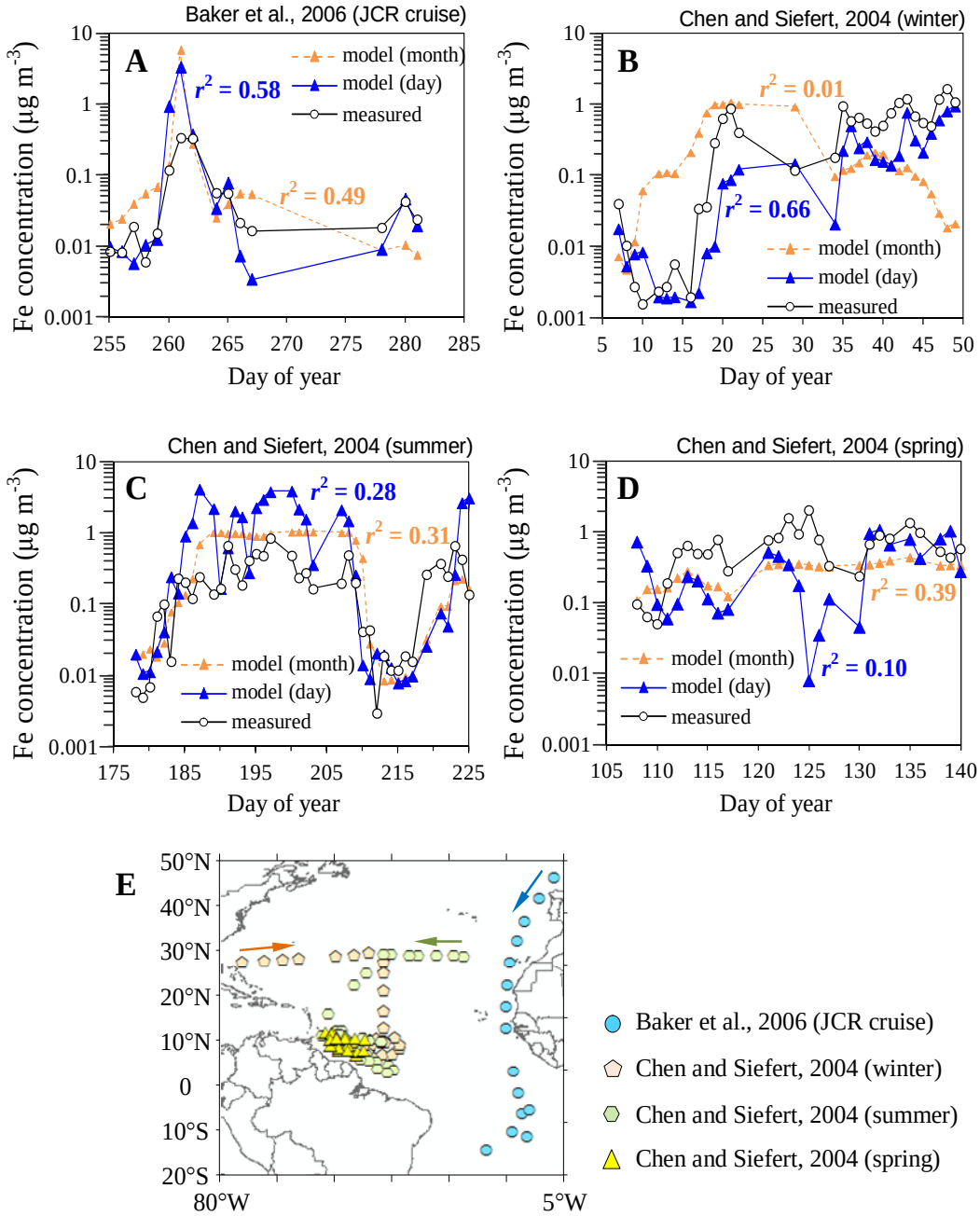

1195

1196

1197

1198

1199 Fig. 9

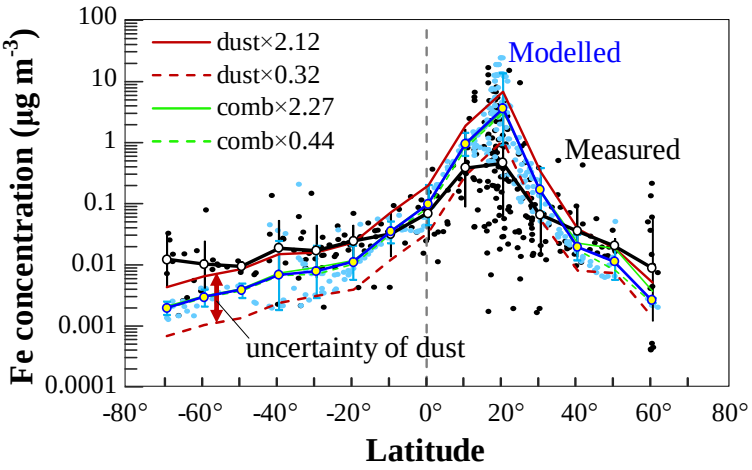

1200

1201

1202 Fig. 10

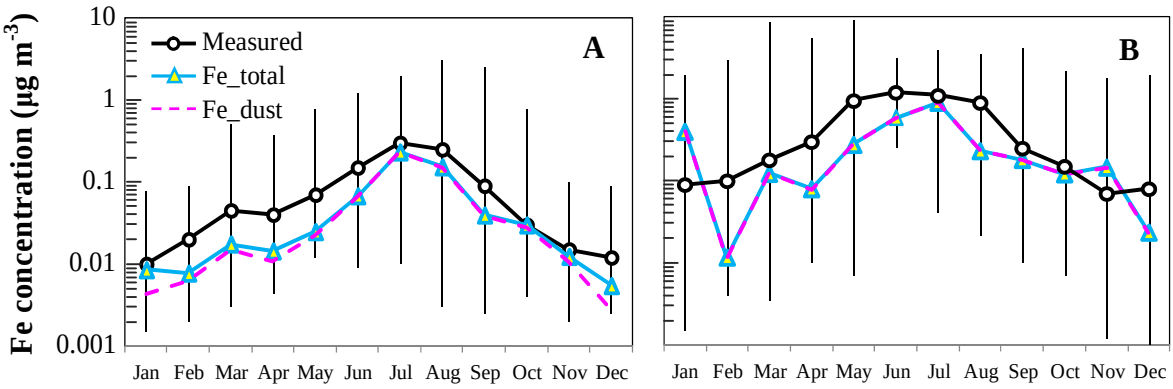

1203

1204

Fig. 11

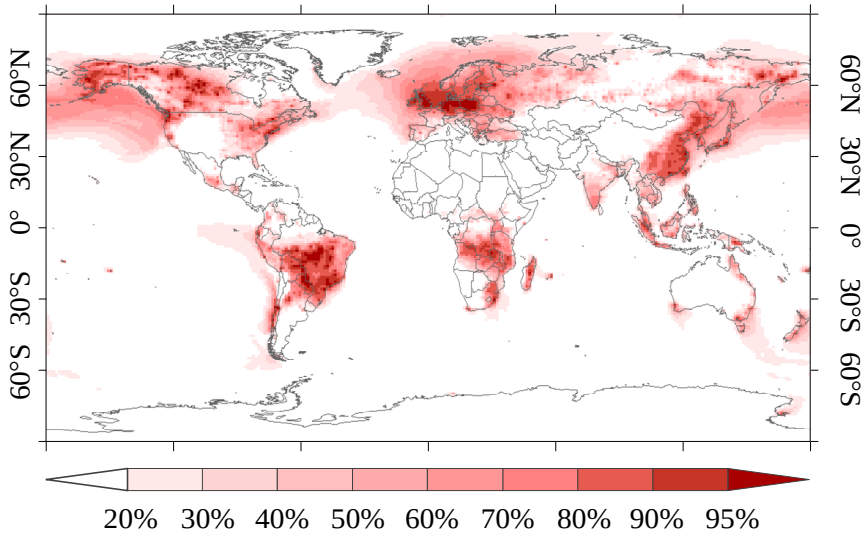

1208 Fig. 12

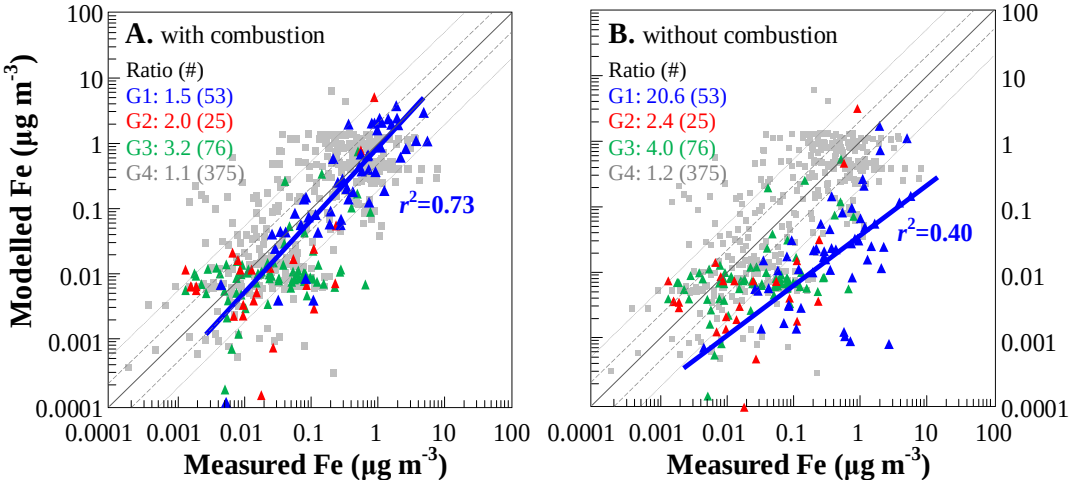

1209

1210

1211 Fig. 13

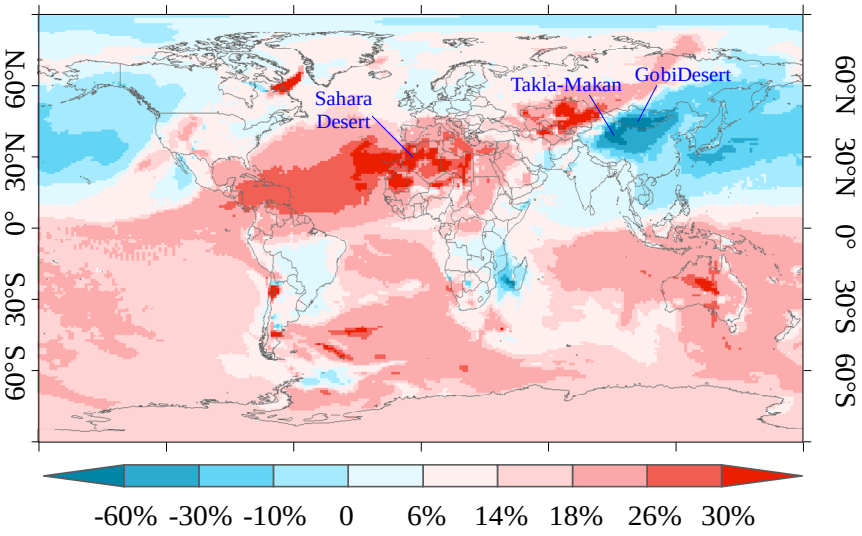

1212

1213

1214 Fig. 14

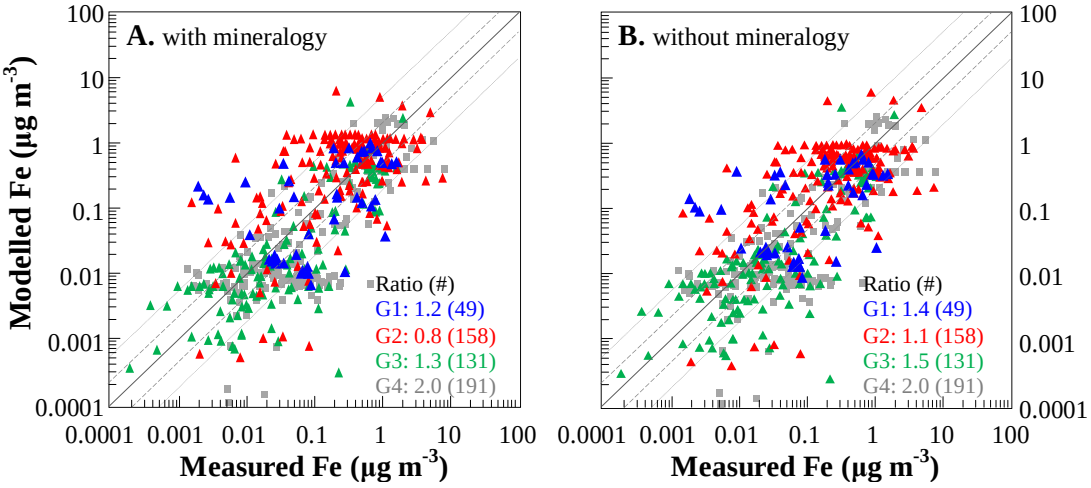

1215

1216

1217 Fig. 15

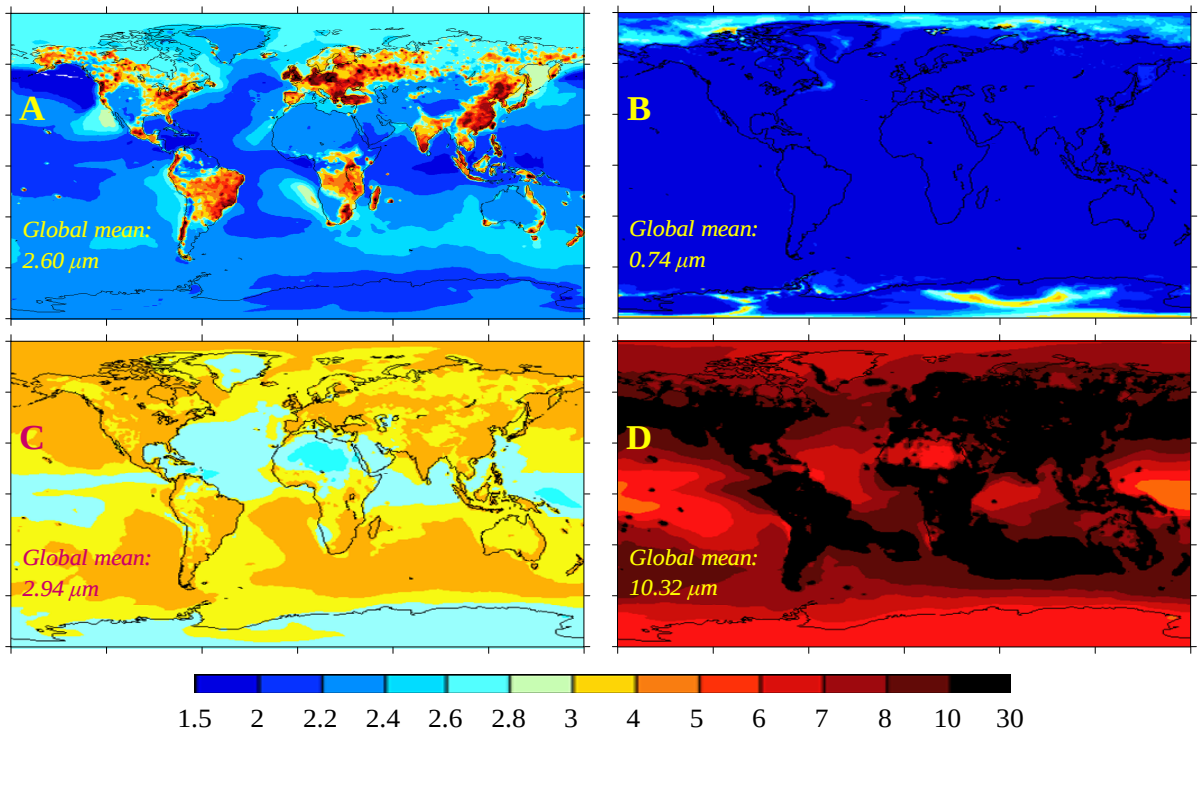

1218

1219

Fig. 16

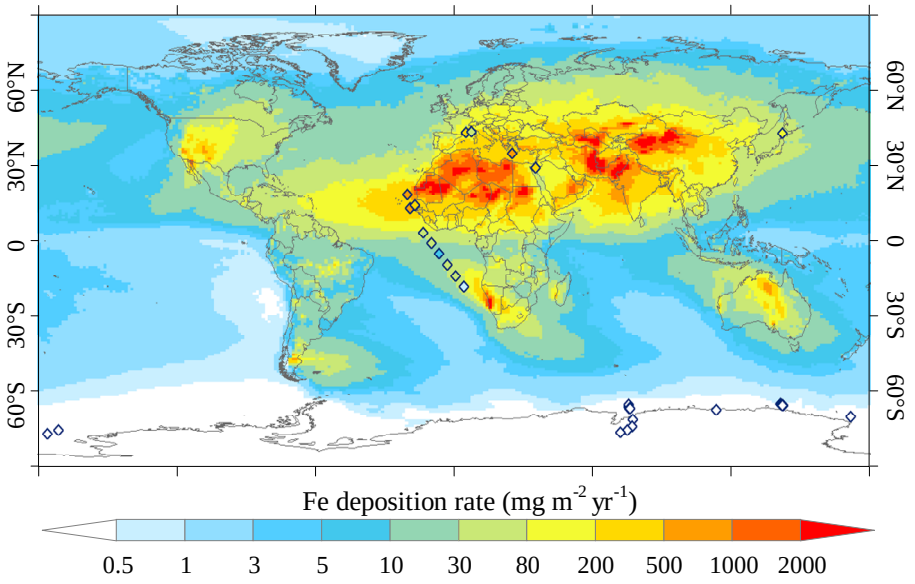
60°N
30°N
0
30°S
60°S
Fe deposition rate (mg m-2 yr-1)
0.5
1
3
5
10
30
80
200
500
1000
2000

Fig. 17

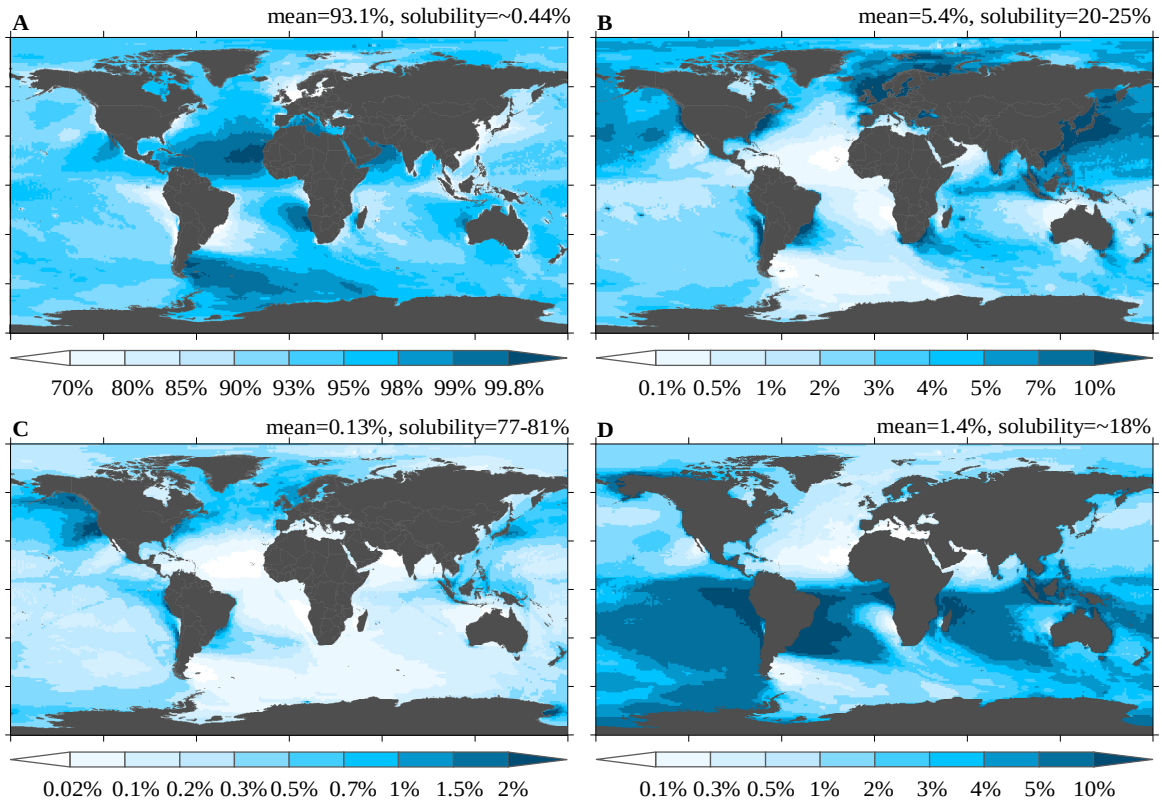
A
mean=93.1%, solubility=~0.44%
70% 80% 85% 90% 93% 95% 98% 99% 99.8%
B
mean=5.4%, solubility=20-25%
0.1% 0.5% 1% 2% 3% 4% 5% 7% 10%
C
mean=0.13%, solubility=77-81%
0.02% 0.1% 0.2% 0.3% 0.5% 0.7% 1% 1.5% 2%
D
mean=1.4%, solubility=~18%
0.1% 0.3% 0.5% 1% 2% 3% 4% 5% 10%

1227 Fig. 18

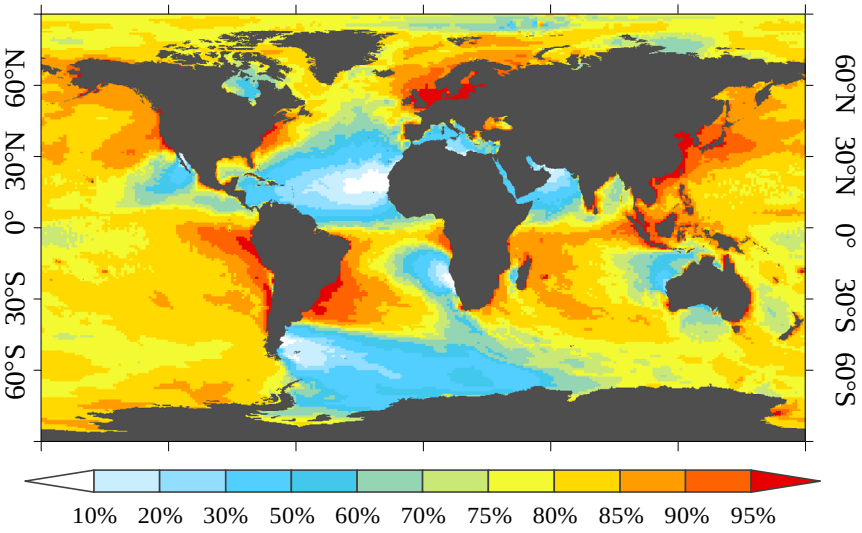

1228

1229

1230 Fig. 19

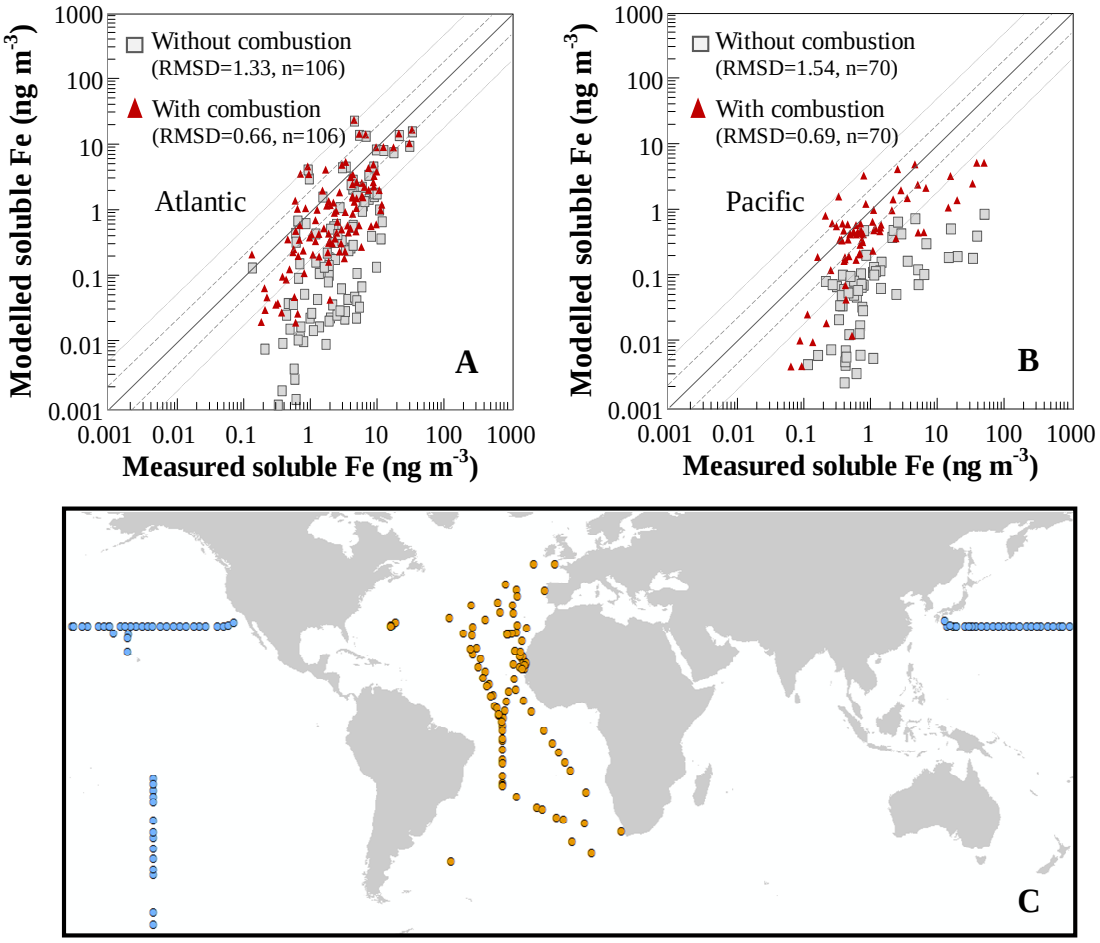

1231